Submission date: 26-May-17

Laminin levels regulate tissue migration and anterior-posterior polarity during egg morphogenesis in *Drosophila*.

María C. Díaz de la Loza[1, 4], Alfonsa Díaz-Torres[1], Federico Zurita[2], Alicia E. Rosales-Nieves[1], Emad Moeendarbary[3, 5], Kristian Franze[3], María D. Martín-Bermudo[1, *] and Acaimo González-Reyes[1, *, #]

[1]Centro Andaluz de Biología del Desarrollo,
CSIC/Universidad Pablo de Olavide/JA,
Carretera de Utrera km 1,
41013 Sevilla,
Spain

[2]Departamento de Genética e Instituto de Biotecnología
Universidad de Granada
Centro de Investigación Biomédica
18071 Granada,
Spain

[3]Department of Physiology, Development and Neuroscience
University of Cambridge
Downing Street
Cambridge CB2 3DY
UK

[4]Current address: Epithelial Biology Laboratory
The Francis Crick Institute
1 Midland Road
London NW1 1AT
UK

[5]Current address: Department of Mechanical Engineering
University College London
London WC1E 7JE
UK

*Correspondence to: MD M-B (e-mail: mdmarber@upo.es; phone: +34-954 348674; fax: +34-954 349376) and AG-R (e-mail: agonrey@upo.es; phone: +34-954 348672; fax: +34-954 349376)

[#]Lead contact

Running head: Laminins control migration and AP polarity.

SUMMARY

Basement membranes (BMs) are specialized extracellular matrices required for tissue organisation and organ formation. We study the role of laminin and its integrin receptor in the regulation of tissue migration during *Drosophila* oogenesis. Egg production in *Drosophila* involves the collective migration of follicle cells (FCs) over the BM to shape the mature egg. We show that laminin contents in the BM increase with time, while integrin amounts in the FCs do not vary significantly. Manipulation of integrin and laminin levels revealed that a dynamic balance of integrin-laminin amounts determines the onset and speed of FC migration. Thus, the interplay of ligand-receptor levels regulates tissue migration *in vivo*. Laminin depletion affects also the ultrastructure and biophysical properties of the BM and results in anterior-posterior misorientation of developing follicles. Laminin emerges as a key player in the regulation of collective cell migration, tissue stiffness and the organisation of anterior-posterior polarity in *Drosophila*.

Key words: collective migration, epithelial migration, laminin, integrin, anterior-posterior polarity, *Drosophila* oogenesis.

INTRODUCTION

Basement membranes (BMs) are specialized types of extracellular matrix (ECM) that coat the basal side of epithelial and endothelial tissues, surround muscles and fat cells and play an active role in tissue and organ morphogenesis (Morrissey and Sherwood, 2015). Most BMs are composed primarily of the secreted glycoproteins laminin, type IV collagen (Col IV), nidogen/entactin and the heparan sulfate proteoglycan perlecan. Alternative proteins that can be found in BMs are papilin, BM-40 or glutactin (Hohenester and Yurchenco, 2013; Yurchenco, 2011). During morphogenesis, BM composition is dynamic and it changes in a temporal and tissue-specific manner to help sculpting organs and tissues (Huang et al., 2003; Rasmussen et al., 2012; Urbano et al., 2009);(Haigo and Bilder, 2011; Harunaga et al., 2014; Pastor-Pareja and Xu, 2011). However, specific functions of the different BM components during morphogenesis remain uncertain.

Egg development in *Drosophila melanogaster* provides an excellent model system to study *in vivo* BM contribution to organogenesis. Adult ovaries are composed of tube-producing eggs termed ovarioles, which show a clear anterior-posterior (AP) polarity. At the anterior tip of each ovariole, a structure called germarium sustains the continuous production of new follicles. Follicles (or egg chambers) consist of 16-germline cell cysts (15 nurse cells and one oocyte) surrounded by the monolayer follicular epithelium. The oocyte is placed posterior to the nurse cells, a step necessary to polarise the developing egg chamber and to allow proper egg fertilisation in the final stages of oogenesis (González-Reyes et al., 1997). During oogenesis, progressively older follicles (classified in 14 stages) remain connected by stalks of specialised follicle cells (FCs) (Spradling, 1993). Stage (S) 1 follicles are

found within the posterior third of the germarium. Once follicles bud off the germarium and until S4, they adopt a spherical appearance. From S5 to S8, egg chambers elongate along the AP axis, becoming ellipsoid in shape. The AP axis of follicles is aligned with that of the ovariole and is determined by the position of the polar cells (Fig. 1A). The apical side of FCs faces the germ line, while their basal surface contacts a BM containing laminin, Col IV, perlecan and nidogen (Gutzeit et al., 1991; Lerner et al., 2013; Lunstrum et al., 1988; Schneider et al., 2006). Follicle elongation is generally linked to FC collective migration, a process termed "global tissue rotation" (Cetera et al., 2014; Gates, 2012; Haigo and Bilder, 2011). During this process, FCs project lamellipodia so that the entire egg chamber rotates in a circular trajectory perpendicular to the AP axis without a discernable leading edge and without affecting the AP alignment of follicles. Rotation is accompanied by the polarised secretion of new ECM material, part of which is eventually deposited in fibrils orientated perpendicular to the follicle's AP axis. These fibrils are thought to create a stiffer ECM in the middle region of the follicle that reinforces the planar polarity of the actin bundles, thus allowing a more efficient collective migration. As a consequence, the follicle's mid-region offers greater resistance to circumferential expansion than to extension along its polar axis, leading to egg elongation (Bilder and Haigo, 2012; Cetera et al., 2014; Gates, 2012; Horne-Badovinac et al., 2012; Isabella and Horne-Badovinac, 2016). However, it has been recently suggested that egg rotation is not a pre-requisite for elongation, as both processes can be uncoupled (Aurich and Dahmann, 2016).

During cell migration, cells adhere and establish traction contacts with their extracellular environment (Friedl and Gilmour, 2009; Reig et al., 2014). Integrins,

transmembrane heterodimeric receptors constituted by the non-covalent association of α and β subunits, are the major mediators in cell-ECM interactions (Hynes, 1992). They link the ECM to the actin cytoskeleton to mediate cell movement and to activate different signalling pathways inside the cell (Wehrle-Haller, 2012; Zaidel-Bar and Geiger, 2010). Follicle rotation implicates the interaction of FCs with the ECM via integrins (Haigo and Bilder, 2011). Laminins, main components of the BM, are well-known integrin ligands and consist of single α, β and γ chains that coil to form a cross-shaped (Beck et al., 1990; Timpl et al., 1979). Once secreted, laminins are proposed to self-assemble through their short arms into networks that recruit the other BM structural components. They remain bonded to the cell surface through the interaction of its long arm with transmembrane receptors, mainly of the integrin family (Hohenester and Yurchenco, 2013; Yurchenco, 2011). Interestingly, the finding that mosaic egg chambers containing laminin-mutant FCs generated round eggs at low frequency suggested that laminins could be involved in FC migration and/or egg chamber elongation (Frydman and Spradling, 2001).

Here we address the role of the balance between integrin and laminin concentrations in epithelial cell migration. By manipulating integrin and laminin levels we find that the dynamics of laminin-integrin levels regulate the timing and speed of collective migration *in vivo*. In addition, we unravel a role for BM composition and stiffness in the maintenance of the egg's AP polarity during oogenesis. As this is a necessary step required for proper fertilisation (Bloch Qazi et al., 2003), our results implicate correct ECM organisation in effective fertilisation.

RESULTS

Laminin depletion results in premature and faster egg chamber rotation.

Drosophila contains two different laminin trimers composed of either of the two α chains, $\alpha_{3,5}$ (encoded by *LanA*) or $\alpha_{1,2}$ (*wing blister*) and the shared β (*LanB1*) and γ chains (*LanB2*) (Chi and Hui, 1989; Graner et al., 1998; Kusche-Gullberg et al., 1992; Montell and Goodman, 1989). To study the pattern of laminin deposition in the ovary we utilised an anti-Laminin β1 polyclonal antibody reported to co-localise with both α laminin subunits in the *Drosophila* embryo and to be specific for Laminin β1 (Kumagai et al., 1997; Urbano et al., 2009). The antibody staining recapitulated laminin α localisation previously described in the germarium and in the BM (Gutzeit et al., 1991; O'Reilly et al., 2008). In summary, Laminin β1 accumulated in the BM that ensheathes the germarium and that is assembled at the basal side of the follicular epithelium from S1 onwards (Fig. 1B, D). Fluorescence quantification revealed that laminin levels doubled from the surface of the germarium to S1 egg chambers, when the follicular epithelium is formed and adopts its monolayer appearance. From then on, laminin accumulates progressively in the BM until it reaches maximum values at S5-S6. During S7-S8, the amount of laminin present in the BM decreases slightly with respect to that of S5-S6 egg chambers (Fig. 1C, E; Table S1).

Making use of the loss of function alleles $LanB1^{28a}$ and *l(2)k05404* (Urbano et al., 2009), we could obtain a hypomorphic condition for the locus with decreased laminin levels. This viable combination gave rise to adult flies (hereafter referred to as *laminin* hypomorphs) that frequently showed a wing blister phenotype, distinctive of *laminin* $\alpha_{1,2}$ and *laminin* $\alpha_{3,5}$ mutants (Henchcliffe et al., 1993; Martin et al., 1999; Woodruff and Ashburner, 1979).

Analysis of *laminin* hypomorphic ovaries confirmed that from S2-S8 laminin levels were kept constant and significantly lower than controls (Fig. 1B, C; Table S1). A similar reduction in Laminin β1 levels was obtained expressing *LanB1* RNAi in the ovary *(tj>LanB1 RNAi)* (Fig. 1D, E). These data confirmed that FCs contribute to the laminin deposited in the ovarian BM and that the *laminin* hypomorphic and the *tj>LanB1 RNAi* conditions are useful tools to decrease laminin levels in oogenesis and particularly during follicle rotation.

The fact that maximum values in laminin deposition are observed during follicle elongation at S5-S6, together with the known involvement of integrins in this process, suggested a role for laminin in collective FC migration and egg elongation (Cetera et al., 2014; Haigo and Bilder, 2011). To test this, we severely decreased *LanB1* and *LanB2* expression in the ovary *(tj>LanB1+LanB2 RNAi)* and found that it gave rise to rounder follicles (100%, n=54) and eggs (86%, n=89; Fig. S1). The appearance of the follicular epithelium was often aberrant, preventing us from assessing in detail the effect of LanB1+LanB2 knock-down on follicle rotation. Thus, laminin is essential for proper egg morphogenesis, a finding supported by the fact that mosaic egg chambers containing FCs mutant for one of the laminin α chains generated round eggs at low frequency (Frydman and Spradling, 2001). Next, we tracked live FCs to determine if a milder reduction in laminin function would affect egg chamber rotation and elongation. We used flies carrying *Fasciclin3::GFP* (*Fas3::GFP*) to mark cell membranes and the position of the polar cells, and *Histone2Av::RFP* (*His2Av::mRFP)* to label chromatin (Fig 2A, B; Movie S1). In agreement with published work (Haigo and Bilder, 2011), all S5-S8 control egg chambers underwent rotation (n=22). In addition, a significant percentage of S2-S4 egg chambers had also initiated rotation (27.8%, n=18) (Fig 2C; see also (Cetera et al.,

2014; Chen et al., 2016). Interestingly, the average rotation speed of control S2-S4 follicles was significantly lower than that of S5-S8 (Fig. 2D; Table S1; Movie S1), which supports the previous proposition that FC migration is reinforced as rotation proceeds (Cetera et al., 2014; Haigo and Bilder, 2011). The low percentage of motile S2-S4 follicles detected in our movies could be due to the inability of two thirds of them to sustain migration or to the fact that S2-S4 egg chambers alternated stationary phases with shorter migratory pulses. To distinguish between these possibilities, we imaged live control ovarioles for long periods (3-6 hours). As a positive control for the imaging conditions, we confirmed that all S5-S6 follicles filmed (n=5) rotated during the entire length of the movies. We filmed S2-S4 follicles (n=9) for a total of 39.6 hours, 21 of which hours corresponded to 3 migrating follicles. Importantly, we never observed rotating follicles that stopped rotation nor stationary ones that initiated migration, strongly suggesting that soon after leaving the germarium, egg chambers either initiate rotation or remain stationary until S5.

laminin hypomorphic and *tj>LanB1 RNAi* egg chambers showed a distinctive behaviour in terms of rotation initiation and speed. In striking contrast to controls, all of the laminin-depleted S2-S4 follicles underwent rotation (n=33; Movies S1 and S2). Further, the average rotation speed of mutant follicles was significantly higher than S2-S4 controls. Similarly, S5-S8 *laminin* hypomorphs and *tj>LanB1 RNAi* rotated faster than controls (Fig. 2D; Table S1). These data confirmed that both the onset and speed of egg chamber rotation *in vivo* depended on specific laminin levels in the BM. In this regard, the degree of variability in laminin deposition observed in S2-S4 control egg chambers might explain their occasional precocious rotation (Fig. 1; Table S1). Finally, in agreement with a recent publication (Chen et

al., 2016), none of the S1 egg chambers analysed from control and laminin-depleted ovaries did rotate (Fig. 2A-C; Movies S1and S2; n=35).

Laminin depletion affects Col IV deposition and BM organisation and stiffness.

The global alignment of actin bundles at the basal side of FCs into planar-polarised arrays perpendicular to the AP axis is maintained and reinforced during follicle rotation at S5-S8. Concomitantly, newly secreted ECM fibrils build a polarized BM necessary for egg morphogenesis (Cetera et al., 2014; Chen et al., 2016; Gates, 2012; Haigo and Bilder, 2011; Isabella and Horne-Badovinac, 2016; Viktorinova and Dahmann, 2013). We set out to determine if laminin was required for actin bundle arrangement and for proper BM assembly and deposition.

First, we visualized actin filaments with rhodamine-labelled phalloidin to test if the premature rotation of young *laminin* hypomorphs was caused by an earlier stimulation of actin bundle polarisation (Fig. S2A and Table S2). Control ovarioles determined that FCs in germaria-S4 follicles (n=56) display a clear polarisation of their basal actin bundles perpendicular to the major axis of the ovariole, even though in S2-S4 follicles it is less prominent (Cetera et al., 2014; Chen et al., 2016). Considering that actin-bundle alignment is detectable in all analysed S2-S4 follicles and that only ~30% of them undergo rotation at these stages, the establishment of tissue-level organisation of actin bundles is independent of follicle rotation. From S5-S6 actin polarisation is gradually enhanced and becomes prominent at S7-S8 (n=49). The observation of *laminin* mutant ovarioles yielded similar results, indicating that the reduction in laminin levels typical of the mutant condition did not

affect the planar polarity of the basal actin cytoskeleton of FCs (n=114).

Second, we analysed whether premature rotation was accompanied by untimely ECM polarisation. We made use of a GFP protein trap in the *viking (vkg)* gene, which codes for the α2 chain of Col IV, and looked at Vkg::GFP deposition in control and mutant ovarioles. While we could detect short Vkg::GFP fibrils in S5-S6 egg chambers, which grew larger and brighter at S7-S8 in both controls and *laminin* hypomorphs, S2-S4 follicles did not present a polarised ECM organisation in either genotype (Fig. S2B and Table S3; n> 35).

Finally, since the laminin network is essential to recruit other BM components during embryonic development (Urbano et al., 2009), we tested whether laminin acted as a scaffold for the deposition of Col IV in the ovary. As reported before, we found low Col IV levels decorating the germarium while its levels increased gradually until they reach a peak at S7-S8 (Isabella and Horne-Badovinac, 2015). On the contrary, *laminin* hypomorphic follicles accumulated lower levels of Col IV, particularly so in S5-S8 follicles (Fig. S3; Table S1). In summary, our results suggest that the main role of laminin in follicle rotation is independent of the establishment of tissue-level planar polarity in migrating FCs. In addition, because precocious migration does not result in fibril orientation prior to S4, continuous follicle rotation is not sufficient for polarised ECM deposition.

To determine in finer detail the consequences for BM organisation of laminin depletion, we analysed BM characteristics using transmission electron microscopy in both control and *laminin* hypomorpic egg chambers. While control follicles displayed a homogeneous BM ~75-100 nm wide, mutant follicles possessed a wider (~115-135 nm) and less compacted BM (Fig. 3A-C). Next, we utilised Atomic Force Microscopy to measure the

apparent elastic modulus *K* as a proxy for BM stiffness (Fig. 3D). To this end, force-distance curves were analysed for an indentation depth of 200 nm, as egg chambers are composite materials with different layers and structures away from the surface further than ~1/10 of the indentation depth do not contribute significantly to *K* (Franze, 2011). We found that control ovarioles are characterised by a significant, continuous increase in BM stiffness soon after follicles leave the germarium. Thus, older follicles possess stiffer BMs than younger ones, at least up to S7-S8. This finding demonstrates a change in BM properties during follicle maturation that coincides with the initiation of consistent tissue rotation. While laminin-depleted follicles also increased stiffness with time, their *K* values at S5-S8 were significantly smaller compared to controls. Taken together, the lower Col IV levels and the less compacted BM observed in laminin hypomorphs most likely reflect the essential role that laminins play in BM assembly, as their polymerisation is a pre-requisite for BM maturation (Hohenester and Yurchenco, 2013).

Integrin levels in FCs influence laminin deposition in the BM.

Our previous results show that FC migration speed increased concomitant to laminin deposition in control ovarioles. However, the strong laminin reduction characteristic of *laminin* hypomorphic or *tj>LanB1 RNAi* ovarioles results in precocious follicle rotation and increased migration speed. These seemingly opposing results prompted us to analyse the role of integrins in FC migration over the BM. Integrins are the main transmembrane receptors that mediate the cell's response to the BM, connecting the ECM with the actin cytoskeleton and activating different signalling pathways (Wickstrom et al., 2011; Zaidel-Bar

and Geiger, 2010). This interaction is essential during cell migration, since integrins are required for the initiation and maturation of adhesion sites, the traction points that allow cell movement through/over the ECM (Galbraith et al., 2007; Wehrle-Haller, 2012). *In vitro*, cell-substratum adhesion can have opposite effects, as it can promote or slow down migration depending on the amount of substrate, integrin expression or activity and integrin-ligand affinity (Palecek et al., 1997). Indeed, depletion of the βPS integrin subunit in FC clones impairs rotation (Haigo and Bilder, 2011), whereas a milder decrease in integrin levels in $mys^{+/-}$ follicles has the opposite effect, increasing rotation speed (Lewellyn et al., 2013). Thus, we investigated if the changes observed in follicle rotation in response to laminin levels depended on integrin expression in the FCs. To this end, we made use of an anti-βPS antibody to determine integrin levels at the basal surface of FCs from germarial stages to S8 in a number of genetic backgrounds (Fig. 4A; Fig. S4A; Table S1). βPS subunit heterodimerizes with αPS1 to form the only functional, laminin-binding integrin expressed from S2-S8 (Devenport and Brown, 2004; Fernandez-Minan et al., 2007). Control ovarioles showed lowest integrin levels in the anterior half of the germarium, maximum levels in S1 follicles and then a relatively constant amount from S2-S8. In the *laminin* hypomorph and in *tj>LanB1 RNAi*, integrin levels were also constant from S2-S8, albeit their levels were consistently lower than controls (between 0.4-0.8-fold of controls; Table S1). Thus, laminin depletion reduces the recruitment of integrin receptors to the basal surface of FCs, confirming that the analysis of follicle rotation should take into account the relative levels of laminin and its integrin receptor αPS1βPS.

We next decreased integrin levels expressing a *mys* RNA interference construct

(*tj>mys RNAi*) in the follicular epithelium and correlated the new integrin amounts with those of laminin. Quantification of the relative integrin amounts confirmed that from S2 to S8 *tj>mys RNAi* FCs accumulated lower integrins at their basal side (0.3-0.6-fold). Surprisingly, laminin deposition in S1-S4 was consistently increased when basal integrin was reduced in *tj>mys RNAi*, while from S5 to S8 it reached control values (Fig. 4; Fig. S4 and Table S1). These data, together with the decrease in integrin levels observed in the *laminin* hypomorphic and *tj>LanB1 RNAi* conditions, indicated that basal localisation of integrins in the follicular epithelium and laminin levels in the adjacent BM are interdependent. Unbeknownst to us the reason for the higher accumulation of laminin in S1-S4 *tj>mys RNAi* egg chambers, the experimental manipulation of integrin levels in the follicular epithelium nonetheless provides the means to elucidate the output of laminin-integrin interactions during collective cell migration in an *in vivo* context.

Laminin levels in the BM and integrin amounts in FCs dictate the onset of rotation and migration speed.

Next we analysed the migratory behaviour of FCs upon genetic manipulation of laminin and integrin levels and reached two major conclusions. First, the onset of follicle rotation at S5 does not depend only on integrin levels, as S2-S3 *tj>mys RNAi* and *laminin* hypomorphic egg chambers contain similar integrin amounts but the former did not show the precocious migration characteristic of the latter. Further, because laminin levels are very different in the above genotypes, it is likely that the interplay between integrin availability and ECM composition dictates the timing of rotation (Fig. 4C; Movie S2; Table S1). Second, cells with

similar integrin amounts but facing BMs with different laminin concentrations migrate at markedly different maximum speeds. Thus, S5-S8 *laminin* hypomorphic and *tj>mys RNAi* egg chambers contain similar integrin levels (~0.5-0.6 -fold of controls in both genotypes) but different laminin amounts (~17 Arbitrary Units [AU] *laminin* hypomorh, ~57 AU *tj>mys RNAi*). Importantly, they differ in their maximum migration speeds (0.62 μm/min and 0.41 μm/min, respectively) (Figs. 2D and 4; Tables S1). Altogether, our results strongly suggest that integrin-ligand levels direct the timing and speed of *in vivo* collective migration. Furthermore, increasing integrin amounts enhanced egg chamber migration speed without affecting the onset of rotation (*tj>ßPS;* Fig. 4; Movies S2 and S3), but the combination of high integrin levels with laminin depletion blocked rotation in 86% of the S2-S6 follicles analysed (n=7) (*tj>lanB1 RNAi + ßPS*. All *tj>lanB1 RNAi + GFP* S2-S6 controls rotated as expected; n=12; Movie S3). To emphasize further that finely tuned cell-ECM interactions regulate collective migration *in vivo*, we found that a reduction in the levels of the structural BM component Col IV caused precocious and faster follicle rotation (Fig. 4C, D; Figure S3; Movie S2; Table S1).

Laminin is required for egg shape and to maintain AP axis alignment.

Given their precocious rotation and faster migration speeds, we wished to determine if egg morphogenesis was affected in *laminin* hypomorphic egg chambers. To this end, we measured the length/width ratio of control eggs which, in agreement with published data, we found to be ~2.75 (Markow et al., 2009) but see (Andersen and Horne-Badovinac, 2016). Mutant eggs laid by *laminin* hypomorphic females did not show any significant differences in length/width ratio with control samples (Fig. 5A, B). Nevertheless, mutant eggs were

significantly shorter and thinner than controls, suggesting that proper egg morphogenesis requires a fully functional BM in the ovary.

The careful analysis of laminin-depleted females showed a novel phenotype in the organisation of the ovariole. The AP axis of developing egg chambers is established early in oogenesis, as shown by the determination of the polar cells at both sides of the developing chamber and by the placement of the oocyte posterior to the sibling nurse cells, in contact with the posterior polar cell cluster (Fig. 1A) (González-Reyes and St Johnston, 1998). Importantly, since the egg chamber's AP axis is aligned with that of the ovariole throughout oogenesis, mature eggs are also orientated along the AP axis, an arrangement that allows fertilisation to occur once the activated egg is lodged into the uterus (Bloch Qazi et al., 2003). In contrast, both *laminin*-hypomorphs and *tj>LanB1 RNAi* females displayed a high proportion of egg chambers in which the oocyte is no longer found at the posterior (Fig. 5C-F). These mispositioned oocytes are not due to the reduction in integrin levels characteristic of laminin-depleted follicles, as *tj>mys RNAi* females do not contain misaligned follicles (n=172). Upon closer examination, two aspects of the oocyte mispositioning phenotype were noted. First, oocyte misplacement was evident only from S4 onwards and the phenotype increased with time. Second, follicles with misplaced oocytes seemed to display a correct AP polarity, as the polar cell clusters were in line with the oocyte. Thus, while follicle AP axis was properly established, it was their alignment with the AP axis of the ovariole that was aberrant (Fig. 5C, D). As a consequence, laminin-depleted ovaries contained eggs with head-to-head or back-to-back orientations, as opposed to the canonical back-to-head arrangements found in control ovaries (Fig. 5F). Of interest, because *vkg* hypomorphic ovaries show precocious

rotation (see above) but did not contained misplaced oocytes (n=98), our results demonstrate that laminin, but not Col IV, is required for proper follicle AP axis alignment.

The finding that oocyte mispositioning is detected after germarial stages suggested that rotation of laminin-depleted follicles was necessary for AP axis misalignment. To test this, we studied two different experimental situations. First, we filmed *laminin*-hypomorphic ovarioles looking for follicles originally aligned with the ovariole's AP axis and that, upon global migration, would deviate their AP axis. We used the position of the posterior interfollicular stalk as a landmark for the original position of the follicle's posterior. In control egg chambers, posterior polar cells and the posterior stalk remain apposed in all cases analysed. On the contrary, we could detect a shift in the relative position of the posterior polar cells and the adjacent stalk in some laminin-depleted follicles (Figs 6A, B; Movies S4 and S5), suggesting that Laminins were essential for proper AP-axis alignment by preventing off-axis rotation of developing follicles. Second, we blocked rotation of laminin-depleted follicles by knocking down the SCAR complex component Abelson interacting protein Abi (Cetera et al., 2014) and analysed AP axis orientation. Control *tj>lanB1 RNAi + GFP* follicles showed 11,3% misplaced oocytes (n=62). Experimental *tj>lanB1 RNAi + Abi RNAi* ovaries displayed a large proportion of malformed follicles in which the follicular epithelium was aberrant. However, in those follicles possessing normal-looking epithelia, the oocyte was placed at the posterior (n=23). Together, the above experiments dictate that a decrease in laminin levels can cause off-axis follicle rotation and, as a consequence, AP axis misalignment.

The axis of rotation is determined by the position of the polar cells.

Live imaging allowed us to detect migrating egg chambers in which their axis of rotation was shifted with respect to that of the ovariole. Since we used the Fas3::GFP line to visualize polar cells in rotating egg chambers, we could determine that the misaligned axes of rotation were in line with the position of the polar cells (Fig. 7A, B; Movie S6). Therefore, since polar cells organize the planar cell polarity of the follicular epithelium (and hence the orientation of lamellipodia) perpendicular to the AP axis (Frydman and Spradling, 2001), polar cells could define the axis of rotation. To test this possibility, we determined that the perpendicular orientation of actin filaments and of Vkg::GFP fibrils was defined by the position of the polar cells in misaligned follicles (Fig. 7C). Second, to rule out the possibility that it was the position of the oocyte what fixed the rotation axis, we imaged follicles mutant for *spindle*-group genes in which the polar cells were aligned with the ovariole's AP axis (González-Reyes et al., 1997) but that contained misplaced oocytes. As shown in Fig. 7D and Movie S7, these egg chambers rotated according to the axis defined by the polar cells. We conclude that it is the position of polar cells and not that of the oocyte that determines the orientation of the rotation axis, most likely by establishing the planar cell polarity of the follicular epithelium.

DISCUSSION

AP egg orientation depends on laminin levels

During normal oogenesis, follicles rotate ~3 complete turns but their axes of rotation do not deviate from their normal AP alignment. Our results show that maintenance of rotation axis orientation requires proper laminin levels, as laminin-depleted ovaries display a significant proportion of misaligned follicles. While mutant S5-S8 follicles possess BMs with altered elastic properties, it is unclear whether this causes rotation axis drift. We envisage that the planar-polarised follicle cell-BM interactions show little variability in a properly assembled, stiff ECM, thus fixing the rotation axis and constraining egg chamber movement. The more elastic BM characteristic of laminin-depleted S5-S8 follicles would allow a higher degree of variability in cell-ECM interactions, resulting often in off-axis rotation. This unexpected function of cell-ECM interactions in the maintenance of AP polarity of developing follicles implicates laminins in the final orientation of mature eggs within the ovary. The positioning of the oocyte at the posterior pole of egg chambers in germarial stages dictates that mature eggs are lodged in the uterus bottom first. As a consequence, the micropyle (the sperm entry site) faces the sperm storage organs seminal receptacle, spermathecae and accessory glands, hence facilitating fertilisation (Bloch Qazi et al., 2003). Considering the significant fraction of misaligned follicles found in laminin-depleted ovaries, physiological levels of laminin are likely to influence fertilisation rate in *Drosophila*. Interestingly, the misalignment phenotype characteristic of mutant follicles suggests that the specific laminin function(s) regulating the onset of rotation do(es) not control rotation axis. The fact that collagen IV-depleted egg chambers also show precocious and faster rotation but do not contain misplaced oocytes

supports this idea.

Regulation of tissue migration by cell-ECM interactions

Mathematical models combined with 2-D or 3-D cell culture experiments (DiMilla et al., 1991; Huttenlocher et al., 1996; Palecek et al., 1997) suggest that maximum migration speed is reached when integrin occupancy by the extracellular substrate leads to an intermediate adhesive strength in which cell traction — required to trigger cell movement — and cell adhesiveness — which slows down migration — are balanced. Thus, migration speed of cells containing a normal pool of integrins showed a biphasic response to the amount of substrate, with maximal velocity at middle levels and a block in migration at higher substrate concentrations. In this system, a decrease in integrin levels augmented the amount of substrate required to reach the maximum speed, emphasizing the importance of integrin-ligand levels in the specification of migration parameters *in vitro*. Our analyses of ligand-receptor interplay during *in vivo* migration of an epithelial sheet extend these and other observations (Gupton and Waterman-Storer, 2006) and support the following conclusions:

1- The dynamic interplay in cellular receptor(s)-extracellular ligand(s) levels regulates the **onset** of collective migration. Because i) both integrins and laminin are essential for rotation, ii) S2-S8 follicles possess constant integrin levels and iii) their ECM becomes stiffer and contains higher laminin levels with time, we propose that the onset of consistent follicular epithelium migration is governed by changes in the ECM. This property is reminiscent of durotaxis, the ability of cells to follow gradients of matrix stiffness (Lo et al., 2000). Further, since reducing integrin and laminin levels as in the hypomorphic condition

initiated rotation precociously in all follicles, the timing of collective migration likely depends not only on changing ECM properties but also on cell receptors-extracellular ligand interactions.

2- Cell-ECM interactions regulate the **speed** of epithelial sheet migration. Considering the equivalent amounts of basal integrins in S2-S8 FCs and assuming that the αPS1 βPS integrin affinity for laminin is similar during these stages, the fact that maximum speed is achieved precisely when laminin levels are highest indicates that laminin concentrations regulate migration speed. This hypothesis is reinforced by the demonstration that high Col IV levels in the BM are required for egg elongation (Isabella and Horne-Badovinac, 2015).

3- The integrin-laminin balance plays a crucial role in the outcome of collective cell migration *in vivo.* Thus, migration speed of FCs with decreased integrin amounts depends on laminin concentration in the BM — the higher the laminin levels, the slower the rotation (i. e., *laminin* hypomorph *versus tj>mys RNAi*). Similarly, over-expression of integrins in laminin-depleted follicles can block migration.

4- In the prevailing model of egg elongation, the polarized deposition of ECM fibrils is a consequence of follicle rotation and requires the polarized secretion of ECM components (Isabella and Horne-Badovinac, 2016). Furthermore, fibril deposition and a concomitant increase in tissue-level actin bundle alignment generate an instructive “molecular corset” that biases egg chamber growth towards the poles (Cetera et al., 2014). Consistent with this model, our results measuring the mechanical properties of developing egg chambers show a marked increase in BM stiffness as rotation proceeds.

5- Continuous, premature rotation in laminin-depleted follicles does not induce

precocious BM polarisation indicating that rotation *per se* is not sufficient to generate a polarised ECM. It most likely requires also Rab10-dependent polarised FC fibril secretion containing Col IV, which we propose starts at S5, coinciding with a significant increase in Rab10 levels and with the initial decrease of Perlecan amounts, assumed to facilitate the "constraining force" of the corset (Isabella and Horne-Badovinac, 2016; Lerner et al., 2013) .

The establishment, stabilisation and disassembly of focal adhesions, the organisation of the actin cytoskeleton and the adhesion between migrating cells are factors known to reinforce migration and to allow collective movement. Our results add to this knowledge and stress that key parameters such as the initiation of collective migration and the speed of migration *in vivo* can be controlled by variations in the levels of ECM ligands and cell receptors. Hence, predicting the response of a cell collective to changes in the ECM ought to contemplate their levels of ECM receptors, as increases in extracellular ligands can have opposite effects on cell behaviours depending on integrin levels. In our model, the ligand-receptor interactions that generate the traction forces required for movement are regulated during development, thus coordinating the timing of tissue growth and morphogenesis. However, our knowledge of the molecular details behind the initiation of collective cell migration is scarce. The findings reported here shed light on the cell biological mechanisms responsible for the initiation of coordinated movement. Considering that cell-ECM interactions are also a hallmark of physiological and pathological conditions that involve cell migration — such as tissue repair, cancer invasion and immunity — the finding that collective migration is regulated by linked cellular and environmental properties broadens our understanding of the cellular basis of development and disease.

EXPERIMENTAL PROCEDURES

Fly stocks

Flies were grown at 25°C on standard medium. *laminin* hypomorphs were trans-heterozygous for *LanB1*^{28a} *(Urbano et al., 2009)* and *l(2)k05404* (Spradling et al., 1999), neither of which affect the coding region. *vkg* hypomorphs were trans-heterozygous for *vkg*^{01209} and *vkg*^{K07138} (Wang et al., 2008). Fas3::GFP (Flybase P[PTT-GA]Fas3G00258; Flytrap G00258), Vkg::GFP (Flybase P[PTT-un1]vkgG205; Flytrap G205), and His2Av::mRFP (Flybase P[His2Av-mRFP1]). The *traffic jam-Gal4* driver *(tj-Gal4*) is expressed in the follicular epithelium and in the epithelial sheath (Andersen and Horne-Badovinac, 2016; Li et al., 2003). To knock-down laminin, Abi or integrin levels in the follicular epithelium, the following lines were used: *UAS-LanB1 RNAi* (VDRC 23119), *UAS-LanB2 RNAi* (VDRC 42559), *UAS-Abi RNAi* (DGRC-Kyoto 9749R) and *UAS-mys RNAi* (VDRC 29619). To overexpress the ßPS integrin subunit we used the *UAS-ßPS* construct (Martin-Bermudo and Brown, 1996). Flies of the appropriate genotype were shifted from 18°C to 25°C for 3 days upon hatching and prior to dissection, except in the case of the *LanB1 RNAi + LanB2 RNAi* experiment, in which flies were shifted to 29°C.

Immunohistochemistry

Antibody, actin and DNA stainings were performed following standard procedures. To analyse laminin, Col IV and integrin levels, experimental and control ovaries were pooled together and treated in parallel. Control ovaries carried the *ubi::GFP* or *His2Av::mRFP* markers (see experimental genotypes in Suppl. Information). Images were acquired with exactly the same settings and quantified in parallel (see below; Fig. S5).

Ex vivo *ovariole culture*

Ovarioles were isolated from ovaries dissected in Schneider medium supplemented with 10% Foetal Bovine Serum (Sigma, F3018), 0.6% (V/V) streptomycin/penicillin antibiotic mix (Invitrogen, 15140-122) and 0.20 mg ml^{-1} insulin (Sigma, 15500) as described previously (Valencia-Exposito et al., 2016). Individual ovarioles without the muscle sheath were transferred to a 35 mm Poly-d-lysine Coated plate (Mattek, P35GC-1.5-10-C) containing supplemented Schneider medium, and let to sink and settle in the bottom of the plate before image acquisition. Although culturing ovarioles *ex-vivo* has been used extensively as a faithful method to study egg morphogenesis during oogenesis, we acknowledge that this is an experimental approach that may not completely reflect egg chamber maturation inside the female's abdomen.

Imaging of fixed and live samples

Images were acquired with a Leica SP5 confocal microscope, analysed utilising Imaris and ImageJ, and processed with Adobe Photoshop and Adobe Illustrator. 3-D images of fixed samples were taken with a 40x/1.3 NA oil immersion objective. 4-D *in vivo* images were obtained at ~20°C. To analyse rotation, a 20x/0.7 NA oil immersion objective and Leica hybrid detectors (standard mode) were used, with time points every 2-4 minutes for 1-6 hours.

Transmission Electron Microscopy protocols and *Atomic Force Microscopy* measurements are detailed in the Suppl. Information section.

Egg shape measurements

Maximum egg length and width of laid eggs from control and *laminin* hypomorph flies were used to calculate the aspect ratio (n=100 for each genotype). Crosses were set with flies of the same age and grown at 25°C following standard procedures.

Data Analysis

Lineal velocity of FCs was calculated by manually tracking nuclei or geometrical cell centres using the Leica LAS AF software. Fluorescence quantification of control and experimental samples was performed on images captured using identical confocal settings (Fig. S5). Quantification of actin bundle and Vkg::GFP fibril alignment was done using the "line ROI" tool of FIJI. See Suppl. Information for further details.

Statistical Analysis

Experiments were performed with at least three biological replicas. Samples were collected from at least 5 different adult females grown at equivalent environmental conditions. The average values ± standard deviations are represented (arbitrary units, AU). P-values were obtained using a Student's t-test to determine values that were significantly different ($P<0.05$).

AUTHOR CONTRIBUTIONS

MCDL, MDM-B and AG-R conceived and designed research; MCDL, AD-T, FZ, AER-N, EM, MDM-B and AG-R performed research; MCDL, AD-T, FZ, EM, KF, MDM-B and AG-R analysed data. MCDL, MDM-B and AG-R wrote the paper.

ACKNOWLEDGMENTS

We thank the BDSC and the VDRC for fly stocks and the DSHB (University of Iowa) for antibodies. The technical support of Beatriz Ibáñez is acknowledged. TEM analysis was performed at the CIC, University of Granada. This work was funded by the Spanish MINECO (Grants BFU2015-65372 to A.G.-R., BFU2013-48988-C2-01 to M.D.M.-B. and Consolider CSD-2007-00008 to M.D.M.-B. and A.G.-R.), by the Junta de Andalucía (Proyecto de Excelencia P09-CVI-5058 to M.D.M.-B. and A.G.-R.) and by the European Regional Development Fund (FEDER). K. F. was supported by a Career Development Award from the UK Medical Research Council. E. M. was supported by a Cambridge Herchel Smith Foundation Fellowship. The help of Kathy García and Lesly Arbesú with image acquisition and analysis is acknowledged.

COMPETING INTERESTS

No competing interests declared.

REFERENCES

Andersen, D., and Horne-Badovinac, S. (2016). Influence of ovarian muscle contraction and oocyte growth on egg chamber elongation in Drosophila. Development *143*, 1375-1387.

Aurich, F., and Dahmann, C. (2016). A Mutation in fat2 Uncouples Tissue Elongation from Global Tissue Rotation. Cell Rep *14*, 2503-2510.

Beck, K., Hunter, I., and Engel, J. (1990). Structure and function of laminin: anatomy of a multidomain glycoprotein. FASEB journal : official publication of the Federation of American

Societies for Experimental Biology *4*, 148-160.

Bilder, D., and Haigo, S.L. (2012). Expanding the morphogenetic repertoire: perspectives from the Drosophila egg. Dev Cell *22*, 12-23.

Bloch Qazi, M.C., Heifetz, Y., and Wolfner, M.F. (2003). The developments between gametogenesis and fertilization: ovulation and female sperm storage in drosophila melanogaster. Developmental Biology *256*, 195-211.

Cetera, M., Ramirez-San Juan, G.R., Oakes, P.W., Lewellyn, L., Fairchild, M.J., Tanentzapf, G., Gardel, M.L., and Horne-Badovinac, S. (2014). Epithelial rotation promotes the global alignment of contractile actin bundles during Drosophila egg chamber elongation. Nature communications *5*, 5511.

Chen, D.Y., Lipari, K.R., Dehghan, Y., Streichan, S.J., and Bilder, D. (2016). Symmetry Breaking in an Edgeless Epithelium by Fat2-Regulated Microtubule Polarity. Cell Rep *15*, 1125-1133.

Chi, H.C., and Hui, C.F. (1989). Primary structure of the *Drosophila* laminin β2 chain and comparison with human, mouse, and *Drosophila* laminin β1 and β2 chains. J Biol Chem *264*, 1543-1550.

Devenport, D., and Brown, N.H. (2004). Morphogenesis in the absence of integrins: mutation of both Drosophila beta subunits prevents midgut migration. Development *131*, 5405-5415.

DiMilla, P.A., Barbee, K., and Lauffenburger, D.A. (1991). Mathematical model for the effects of adhesion and mechanics on cell migration speed. Biophysical journal *60*, 15-37.

Fernandez-Minan, A., Martin-Bermudo, M.D., and Gonzalez-Reyes, A. (2007). Integrin signaling regulates spindle orientation in Drosophila to preserve the follicular-epithelium monolayer. Curr Biol *17*, 683-688.

Franze, K. (2011). Atomic force microscopy and its contribution to understanding the development of the nervous system. Curr Opin Genet Dev *21*, 530-537.

Friedl, P., and Gilmour, D. (2009). Collective cell migration in morphogenesis, regeneration and cancer. Nat Rev Mol Cell Biol *10*, 445-457.

Frydman, H.M., and Spradling, A.C. (2001). The receptor-like tyrosine phosphatase lar is required for epithelial planar polarity and for axis determination within *Drosophila* ovarian follicles. Development *128*, 3209-3220.

Galbraith, C.G., Yamada, K.M., and Galbraith, J.A. (2007). Polymerizing actin fibers position

integrins primed to probe for adhesion sites. Science *315*, 992-995.

Gates, J. (2012). Drosophila egg chamber elongation: insights into how tissues and organs are shaped. Fly (Austin) *6*, 213-227.

González-Reyes, A., Elliott, H., and St Johnston, D. (1997). Oocyte determination and the origin of polarity in Drosophila: the role of the spindle genes. Development *124*, 4927-4937.

González-Reyes, A., and St Johnston, D. (1998). The *Drosophila* AP axis is polarised by the cadherin-mediated positioning of the oocyte. Development *125*, 3635-3644.

Graner, M.W., Bunch, T.A., Baumgartner, S., Kerschen, A., and Brower, D.L. (1998). Splice variants of the *Drosophila* PS2 integrins differentially interact with RGD-containing fragments of the extracellular proteins tiggrin, ten-m, and D-laminin α2. J Biol Chem *273*, 18235-18241.

Gupton, S.L., and Waterman-Storer, C.M. (2006). Spatiotemporal feedback between actomyosin and focal-adhesion systems optimizes rapid cell migration. Cell *125*, 1361-1374.

Gutzeit, H.O., Eberhardt, W., and Gratwohl, E. (1991). Laminin and basement membrane-associated microfilaments in wild-type and mutant Drosophila ovarian follicles. J Cell Sci *100 (Pt 4)*, 781-788.

Haigo, S.L., and Bilder, D. (2011). Global tissue revolutions in a morphogenetic movement controlling elongation. Science *331*, 1071-1074.

Harunaga, J., Doyle, A., and Yamada, K. (2014). Local and global dynamics of the basement membrane during branching morphogenesis require protease activity and actomyosin contractility. Dev Biol *394*, 197-205.

Henchcliffe, C., García-Alonso, L., Tang, J., and Goodman, C.S. (1993). Genetic analysis of laminin A reveals diverse functions during morphogenesis in *Drosophila*. Development *118*, 325-337.

Hohenester, E., and Yurchenco, P.D. (2013). Laminins in basement membrane assembly. Cell Adh Migr *7*, 56-63.

Horne-Badovinac, S., Hill, J., Gerlach, G., 2nd, Menegas, W., and Bilder, D. (2012). A screen for round egg mutants in Drosophila identifies tricornered, furry, and misshapen as regulators of egg chamber elongation. G3 (Bethesda) *2*, 371-378.

Huang, C., Rajfur, Z., Borchers, C., Schaller, M., and Jacobson, K. (2003). JNK phosphorylates paxillin and regulates cell migration. Nature *424*, 219-223.

Huttenlocher, A., Ginsberg, M.H., and Horwitz, A.F. (1996). Modulation of cell migration by integrin-mediated cytoskeletal linkages and ligand-binding affinity. J Cell Biol *134*, 1551-1562.

Hynes, R.O. (1992). Integrins: versatility, modulation, and signaling in cell adhesion. Cell *69*, 11-25.

Isabella, A.J., and Horne-Badovinac, S. (2015). Dynamic regulation of basement membrane protein levels promotes egg chamber elongation in Drosophila. Dev Biol *406*, 212-221.

Isabella, A.J., and Horne-Badovinac, S. (2016). Rab10-Mediated Secretion Synergizes with Tissue Movement to Build a Polarized Basement Membrane Architecture for Organ Morphogenesis. Dev Cell *38*, 47-60.

Kumagai, C., Kadowaki, T., and Kitagawa, Y. (1997). Disulfide-bonding between *Drosophila* laminin β and γ chains is essential for α chain to form $\alpha\beta\gamma$ trimer. FEBS Lett *412*, 211-216.

Kusche-Gullberg, M., Garrison, K., MacKrell, A.J., Fessler, L.I., and Fessler, J.H. (1992). Laminin A chain: expression during Drosophila development and genomic sequence. EMBO J *11*, 4519-4527.

Lerner, D.W., McCoy, D., Isabella, A.J., Mahowald, A.P., Gerlach, G.F., Chaudhry, T.A., and Horne-Badovinac, S. (2013). A Rab10-dependent mechanism for polarized basement membrane secretion during organ morphogenesis. Dev Cell *24*, 159-168.

Lewellyn, L., Cetera, M., and Horne-Badovinac, S. (2013). Misshapen decreases integrin levels to promote epithelial motility and planar polarity in Drosophila. J Cell Biol *200*, 721-729.

Li, M.A., Alls, J.D., Avancini, R.M., Koo, K., and Godt, D. (2003). The large Maf factor Traffic Jam controls gonad morphogenesis in *Drosophila*. Nat Cell Biol *5*, 994-1000.

Lo, C.M., Wang, H.B., Dembo, M., and Wang, Y.L. (2000). Cell movement is guided by the rigidity of the substrate. Biophysical journal *79*, 144-152.

Lunstrum, G., Baechinger, H.-P., Fessler, L.I., Duncan, K., Nelson, R., and Fessler, J. (1988). Drosophila basement membrane procollagen IV. I. Protein characterization and distribution. J BiolChem *263*, 18318-18327.

Markow, T.A., Beall, S., and Matzkin, L.M. (2009). Egg size, embryonic development time and ovoviviparity in Drosophila species. J Evol Biol *22*, 430-434.

Martin, D., Zusman, S., Li, X., Williams, E.L., Khare, N., DaRocha, S., Chiquet-Ehrismann, R., and Baumgartner, S. (1999). wing blister, a new *Drosophila* laminin alpha chain required for

cell adhesion and migration during embryonic and imaginal development. J Cell Biol *145*, 191-201.

Martin-Bermudo, M.D., and Brown, N.H. (1996). Intracellular signals direct integrin localization to sites of function in embryonic muscles. J Cell Biol *134*, 217-226.

Montell, D.J., and Goodman, C.S. (1989). Drosophila laminin: sequence of B2 subunit and expression of all three subunits during embryogenesis. J Cell Biol *109*, 2441-2453.

Morrissey, M.A., and Sherwood, D.R. (2015). An active role for basement membrane assembly and modification in tissue sculpting. J Cell Sci *128*, 1661-1668.

O'Reilly, A.M., Lee, H.H., and Simon, M.A. (2008). Integrins control the positioning and proliferation of follicle stem cells in the Drosophila ovary. J Cell Biol *182*, 801-815.

Palecek, S.P., Loftus, J.C., Ginsberg, M.H., Lauffenburger, D.A., and Horwitz, A.F. (1997). Integrin-ligand binding properties govern cell migration speed through cell-substratum adhesiveness. Nature *385*, 537-540.

Pastor-Pareja, J.C., and Xu, T. (2011). Shaping cells and organs in Drosophila by opposing roles of fat body-secreted Collagen IV and perlecan. Dev Cell *21*, 245-256.

Rasmussen, J.P., Reddy, S.S., and Priess, J.R. (2012). Laminin is required to orient epithelial polarity in the C. elegans pharynx. Development *139*, 2050-2060.

Reig, G., Pulgar, E., and Concha, M.L. (2014). Cell migration: from tissue culture to embryos. Development *141*, 1999-2013.

Schneider, M., Khalil, A.A., Poulton, J., Castillejo-Lopez, C., Egger-Adam, D., Wodarz, A., Deng, W.M., and Baumgartner, S. (2006). Perlecan and Dystroglycan act at the basal side of the Drosophila follicular epithelium to maintain epithelial organization. Development *133*, 3805-3815.

Spradling, A. (1993). Developmental genetics of oogenesis. In The Development of Drosophila melanogaster, M. Bate, and A. Martinez-Arias, eds. (New York: Cold Spring Harbor Laboratory press), pp. 1-70.

Spradling, A., Stern, D., Beaton, A., Rhem, E., Laverty, T., Mozden, N., Misra, S., and Rubin, G. (1999). The Berkeley Drosophila Genome Project Gene Disruption Project: Single P- Element insertions mutating 25% of vital Drosophila genes. Genetics *153*, 135- 177.

Timpl, R., Rohde, H., Robey, P.G., Rennard, S.I., Foidart, J.M., and Martin, G.R. (1979).

Laminin--a glycoprotein from basement membranes. J Biol Chem *254*, 9933-9937.

Urbano, J.M., Torgler, C.N., Molnar, C., Tepass, U., Lopez-Varea, A., Brown, N.H., de Celis, J.F., and Martin-Bermudo, M.D. (2009). Drosophila laminins act as key regulators of basement membrane assembly and morphogenesis. Development *136*, 4165-4176.

Valencia-Exposito, A., Grosheva, I., Miguez, D.G., Gonzalez-Reyes, A., and Martin-Bermudo, M.D. (2016). Myosin light-chain phosphatase regulates basal actomyosin oscillations during morphogenesis. Nature communications *7*, 10746.

Viktorinova, I., and Dahmann, C. (2013). Microtubule polarity predicts direction of egg chamber rotation in Drosophila. Curr Biol *23*, 1472-1477.

Wang, X., Harris, R.E., Bayston, L.J., and Ashe, H.L. (2008). Type IV collagens regulate BMP signalling in Drosophila. Nature *455*, 72-77.

Wehrle-Haller, B. (2012). Assembly and disassembly of cell matrix adhesions. Curr Opin Cell Biol *24*, 569-581.

Wickstrom, S.A., Radovanac, K., and Fassler, R. (2011). Genetic analyses of integrin signaling. Cold Spring Harb Perspect Biol *3*.

Woodruff, R.C., and Ashburner, M. (1979). The genetics of a small autosomal region of *Drosophila* melanogaster containing the structural gene for alcohol dehydrogenase. II. Lethal mutations in the region. Genetics *92*, 133-149.

Yurchenco, P.D. (2011). Basement membranes: cell scaffoldings and signaling platforms. Cold Spring Harb Perspect Biol *3*.

Zaidel-Bar, R., and Geiger, B. (2010). The switchable integrin adhesome. J Cell Sci *123*, 1385-1388.

FIGURE LEGENDS

Figure 1: **Quantification of laminin levels in *laminin*-depleted ovaries. (A)** Schematic representation of an ovariole. **(B, D)** Immunodetection of the Laminin ß1 subunit in control, *laminin* hypomorphic and *tj>LanB1 RNAi* ovarioles. Images are maximum Z-projections of at least 15 sections. **(C, E)** Quantification of the immunofluorescence signal. Mean and standard deviation (SD) of at least 14 measurements per genotype and stage are indicated. In this and the rest of figures: anterior is to the left; g: germarium; S: oogenesis stages; P values of two-tailed t-tests <0.05 were considered statistically significant (*: P<0.05, **: P<0.005, ***: P<0.001). See Table S1, Fig. S1. Scale bars = 25 microns.

Figure 2: Laminin ß1-depleted ovarioles show premature and faster egg chamber rotation. **(A)** Time lapse of a control ovariole. **(B)** Time lapse of a *laminin* hypomorphic ovariole. **(C)** Quantification of rotating egg chambers in control and Laminin β1-depleted ovarioles. Values above boxes indicate the number of egg chambers analysed. **(D)** Quantification of the rotation speeds. Horizontal lines in boxes represent MEDIAN values of a minimum of 23 and a maximum of 103 measurements per genotype and stage. Values above boxes indicate MEAN rotation speeds. See Movie S1, Table S1 for SD values and Figs. S1-S3. Scale bars = 25 microns.

Figure 3: Laminin depletion causes ultra-structural and biophysical changes in the BM. Transmission electron microscopy images of the basal side of S4-S5 control **(A)** and *laminin*-hypomorphic **(B)** FCs. The BM is indicated with white brackets. **(C)** Quantification of BM

width. The graph corresponds to a minimum of 21 and a maximum of 44 measurements per genotype and stage. **(D)** Comparison of the apparent elastic modulus *K* at discrete points along control (58 measurements from 11 ovarioles) and *laminin* hypomorph mutant ovarioles (48 measurements from 10 ovarioles) ex vivo. Results shown refer to an indentation depth of 0.2 μm to reflect BM properties. Statistically significant increases in *K* shown in the graph correspond to control *vs* mutant tissue of the same stage. The table refers to the comparison between follicles of the same genotype but of different stage. Horizontal lines in boxes represent MEDIAN values; Xs indicate MEAN values. n. s.: not significant (P>0.05; two-tailed t-test). See Table S1. Error bars: SD.

Figure 4: Integrin and laminin levels and rotation speeds. Quantification of the immunofluorescence signal of **(A)** anti-ßPS and **(B)** anti-Laminin ß1 antibodies. Mean and SD values from 3 to 5 ovarioles per genotype are plotted. **(C)** Onset of rotation and **(D)** quantification of rotation speed at different stages. Horizontal lines in boxes represent MEDIAN values of a minimum of 11 and a maximum of 103 measurements per genotype and stage. Values above boxes indicate MEAN rotation speeds. See Figs. S4, S5 and Movies S1, S2.

Figure 5: Laminin depletion results in egg chamber AP axis misalignment. (A) Eggs laid by control and *laminin* hypomorphic females**. (B)** Quantification of length, width and aspect ratio. Control eggs: 525±15.5 μm length, 190±6.85 μm width, aspect ratio = 2.74±0.20; *lam* hypomorfic eggs: 493±16.8 μm length, 181±11.4 μm width, aspect ratio = 2.76±0.13. Mean and SD are shown (n=100 per each genotype). ns: not significant (P>0.05). **(C)** The oocyte

(labelled in green; white asterisk) is found at the posterior of S1-S4 control and *laminin* hypomorph follicles. At later stages, a fraction of *laminin* hypomorphs shows oocytes misaligned with the ovariole's AP axis. **(D)** The Fas3 marker labels the position of the anterior and posterior polar cells (white brackets). In controls, polar cells align with the ovariole's AP axis (yellow arrows). Laminin-depleted egg chambers display polar cells misaligned with the ovariole's axis. In both controls and laminin-depleted follicles, the oocyte is always adjacent to the posterior polar cells. **(E)** Quantification of the frequency of misplaced oocytes. Control follicles displayed 100% posterior oocytes (n=259). The number of follicles analysed is shown. **(F)** Mature eggs found in control ovarioles are always posterior first (white arrows). *laminin* hypomorphic ovarioles can display mature eggs with a reverse polarity (red arrows), resulting in head-to-head or back-to-back orientations (A: anterior end of ovariole; P: posterior end). Asterisks: oocytes. Scale bars = 25 microns, except in **(A, F)**, which is 250 microns.

Figure 6: Oocyte misplacement in laminin-depleted ovaries as a result of egg chamber rotation. Time lapse movies of control and *laminin* hypomorphic follicles carrying the histone marker His2Av::mRFP and the polar cell marker Fas::GFP. **(A, A')** Controls maintain the alignment of posterior polar cells (yellow dotted line) and the interfollicular stalk (blue dotted line) during rotation. **(B, B')** In contrast, in *laminin* hypomorphs, posterior polar cells and stalk cells can separate during rotation. The separation of the posterior polar cells from the stalk is limited (white arrow), but it is worth mentioning that the movie lasts only 1/10th of the total rotation from S5 to S8. See Movies S4, S5. Scale bars = 25 microns.

Figure 7: The position of the polar cells, but not of the oocyte, determines the axis of rotation. Time lapse analysis of control **(A)** and *laminin* hypomorphic **(B)** ovarioles labelled with His2Av::mRFP to mark nuclei and Fas3::GFP to outline FCs and polar cells. **(C)** Cross-section and surface view of a misaligned S6 egg chamber from a *laminin* hypomorph carrying the Vkg::GFP protein trap to label ECM fibrils and stained with rhodamine-labelled phalloidin to visualise basal actin filaments. **(D)** Phase-contrast image of a *spindle-C spindle-A* double mutant egg chamber carrying a misplaced oocyte, as shown by the position of the oocyte's nucleus (Oo, arrow and asterisk). Brackets mark the presumptive position of the polar cells. **(E)** Time lapse analysis of the rotation axis (dashed line), which is defined by the position of the polar cells. See Movies S4, S6, S7. Scale bars in A, B and D = 25 microns; in C = 5 microns. Outlined cells are used to monitor rotation.

SUPPLEMENTAL MOVIES

Supplemental Movie 1 (related to Fig. 2): Egg chamber rotation in control and *laminin* hypomorphic ovarioles. Confocal images of egg chambers from the same ovariole were arranged with their anterior to the left. Follicle cells, including the brighter polar cells, are labelled with Fasciclin3::GFP (Fas3::GFP; green). Histone::RFP (His2Av:mRFP; red) marks chromatin. Control egg chambers rotate predominantly from S5 to S8. In all cases analysed, rotation in *laminin* hypomorphs is detected from S2 to S8. Scale bar = 25 microns.

Supplemental Movie 2 (related to Figs. 2 and 4): Egg chamber rotation in *tj>LanB1 RNAi, tj>mys RNAi, tj>ßPS* and *vkg* hypomorphic ovarioles. Transmitted-light images from

ovarioles of different genotypes were acquired using phase contrast. Follicles from the same ovariole were arranged with their anterior to the left. The position of nuclei and cell outlines were used to calculate rotation speed. Scale bar = 25 microns.

Supplemental Movie 3 (related to Fig. 4): Egg chamber rotation in *tj> LanB1 RNAi*, *tj>ßPS* and *tj> LanB1 RNAi + ßPS* ovarioles. Transmitted-light images of individual egg chambers of the above genotypes were acquired using phase contrast. The position of nuclei and cell outlines were used to verify rotation (or the absence of, in the case of *tj> LanB1 RNAi + ßPS)*. Scale bar = 25 microns.

Supplemental Movie 4 (related to Figs. 6 and 7): Egg chamber rotation in a control ovariole. Follicle cells, including the brighter polar cells, are labelled with Fasciclin3::GFP (Fas3::GFP). Histone::RFP (His2Av:mRFP) marks chromatin. Control egg chambers rotate predominantly from S5 to S8. Scale bar = 25 microns.

Supplemental Movie 5 (related to Fig. 6): Egg chamber rotation in a *laminin* hypomorphic ovariole carrying a misaligned egg chamber. Follicle cells, including the brighter polar cells, are labelled with Fasciclin3::GFP (Fas3::GFP). Histone::RFP (His2Av:mRFP) marks chromatin. The distance between the posterior polar cells and the stalk cells of a S6 egg chamber increases with time. Scale bar = 25 microns.

Supplemental Movie 6 (related to Fig. 7): Egg chamber rotation in a *laminin* hypomorphic

ovariole. Follicle cells, including the brighter polar cells, are labelled with Fasciclin3::GFP (Fas3::GFP). Histone::RFP (His2Av:mRFP) marks chromatin. Follicle cell tracking of a misaligned egg chamber in a *laminin* hypomorphic S6 egg chamber. The axis of rotation is established by the position of the polar cells. Scale bar = 25 microns.

Supplemental Movie 7 (related to Fig. 7): Time lapse of a *spindle* double mutant egg chamber (*spn-C*^{094} *spn-A*^{057}) carrying a misplaced oocyte. Transmitted-light images were acquired using phase contrast. Scale bar = 25 microns.

Fig. 1

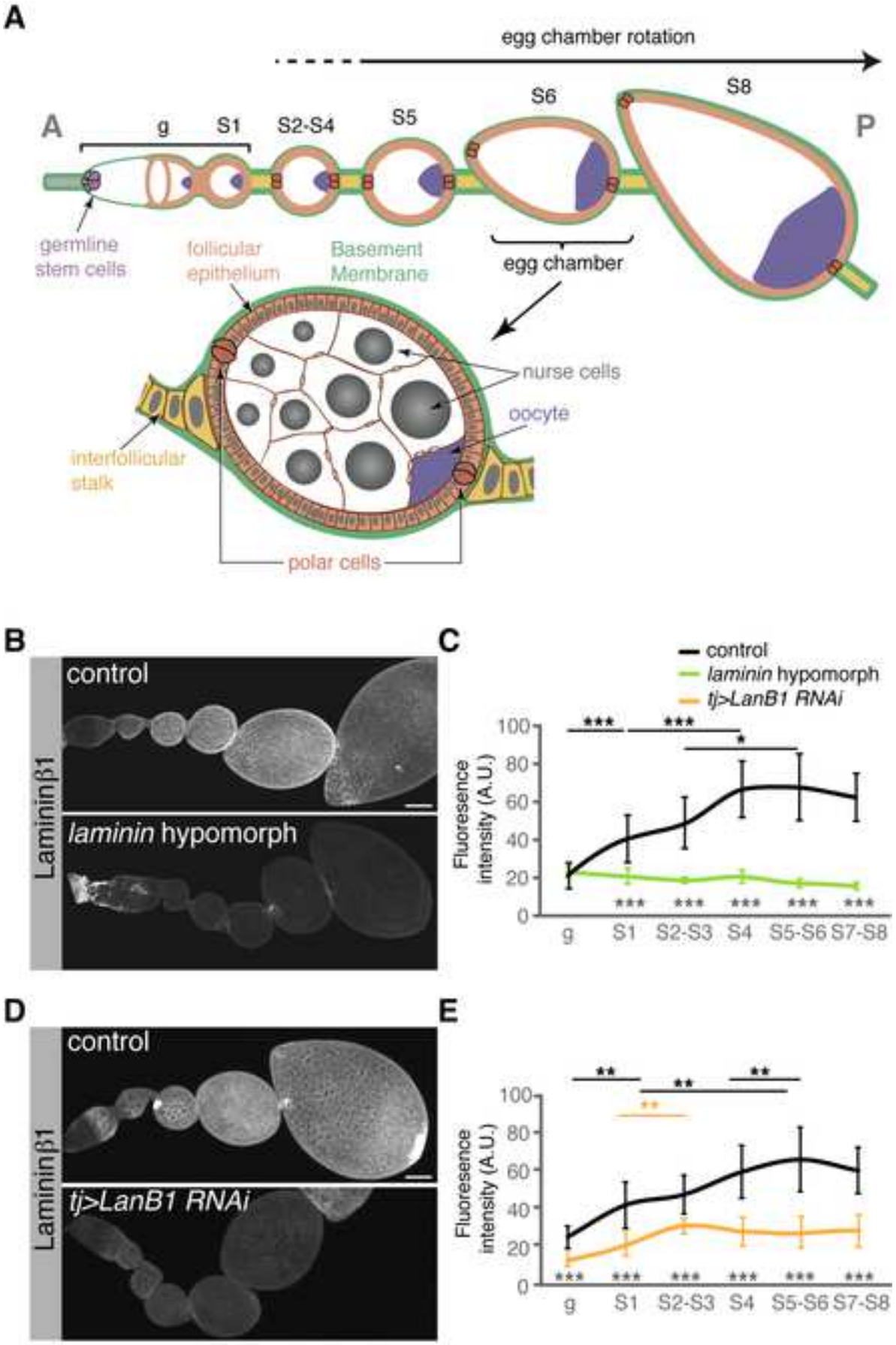

Figure 1

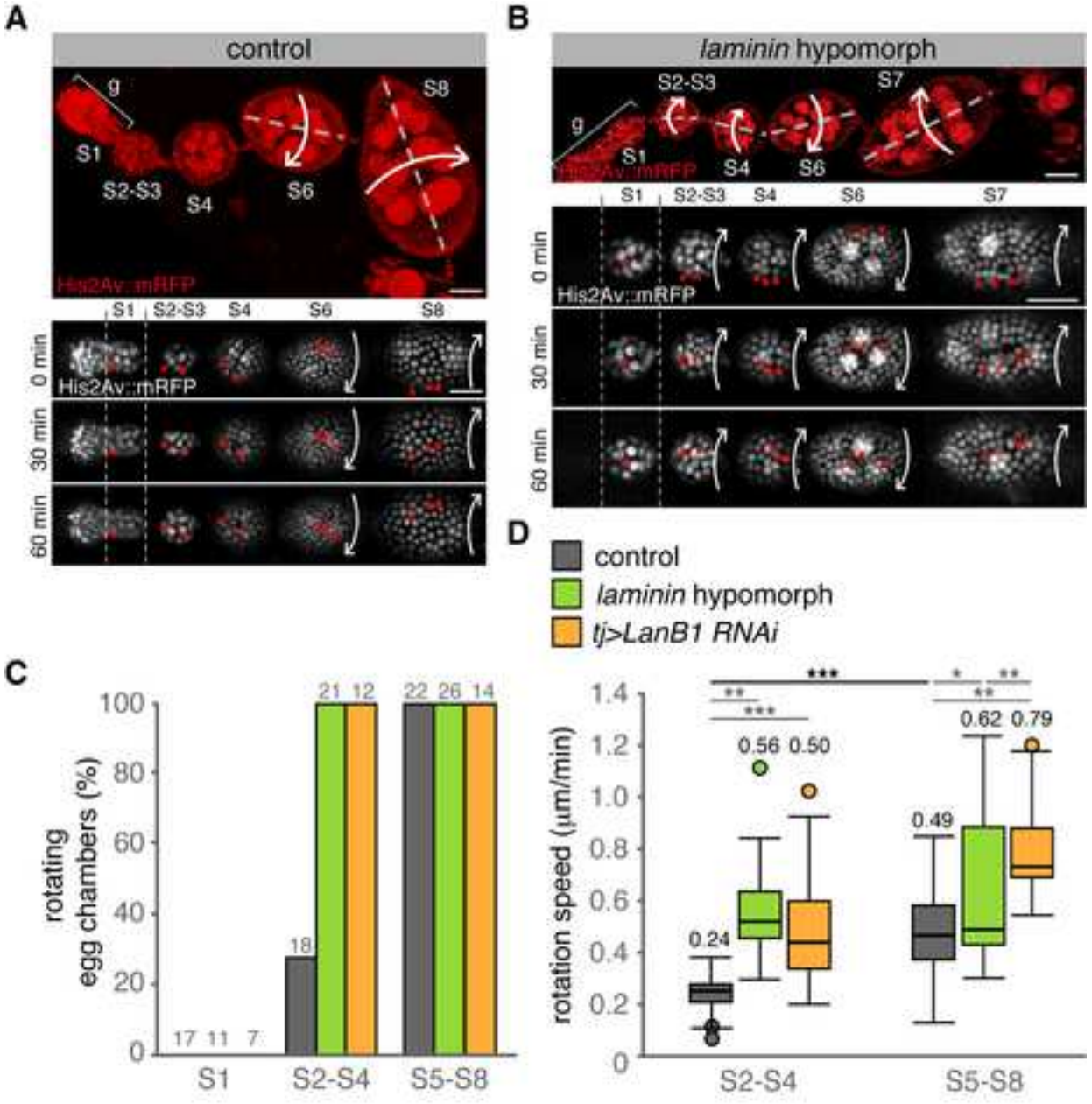

Figure 2

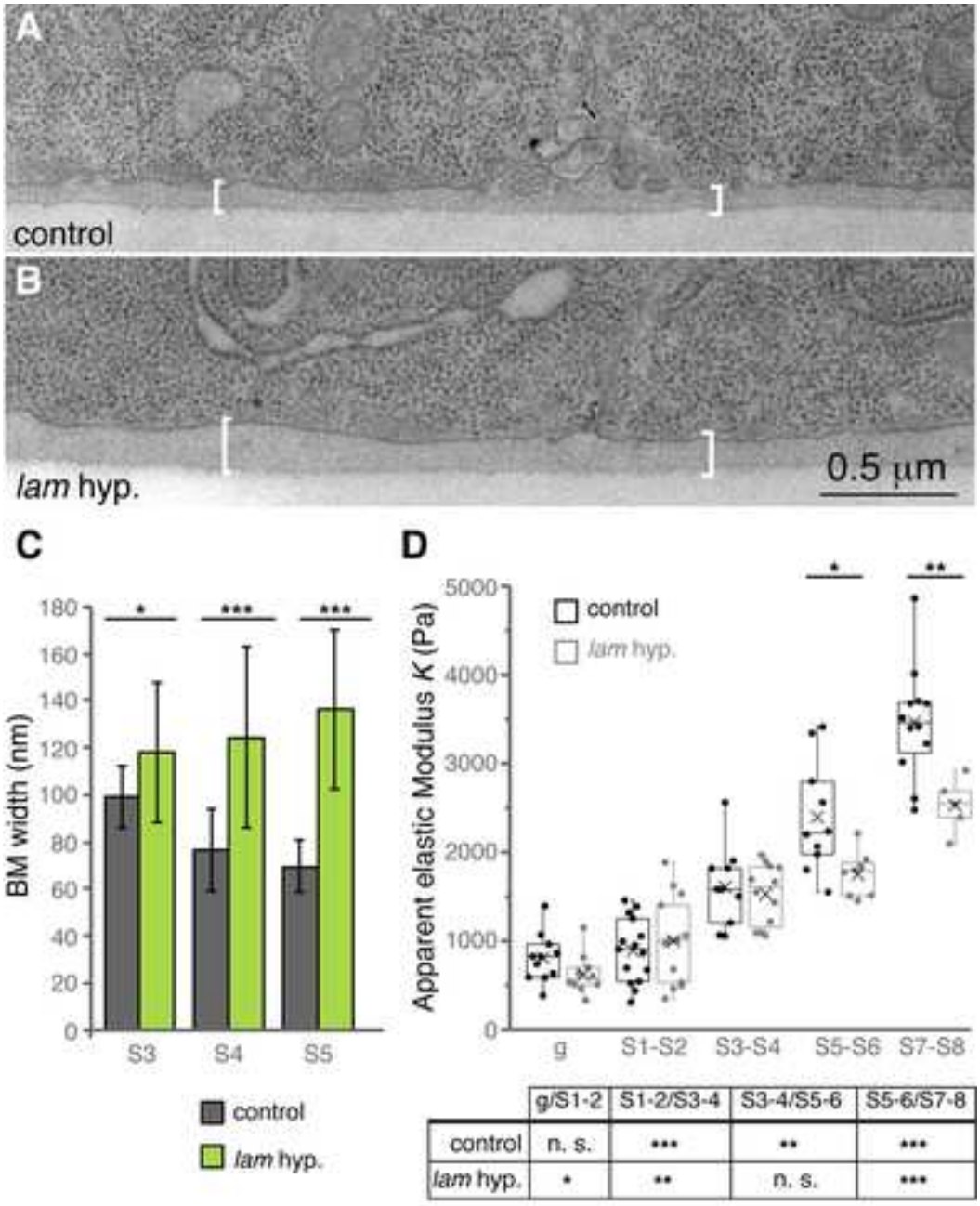

	g/S1-2	S1-2/S3-4	S3-4/S5-6	S5-6/S7-8
control	n. s.	***	**	***
lam hyp.	*	**	n. s.	***

Figure 3

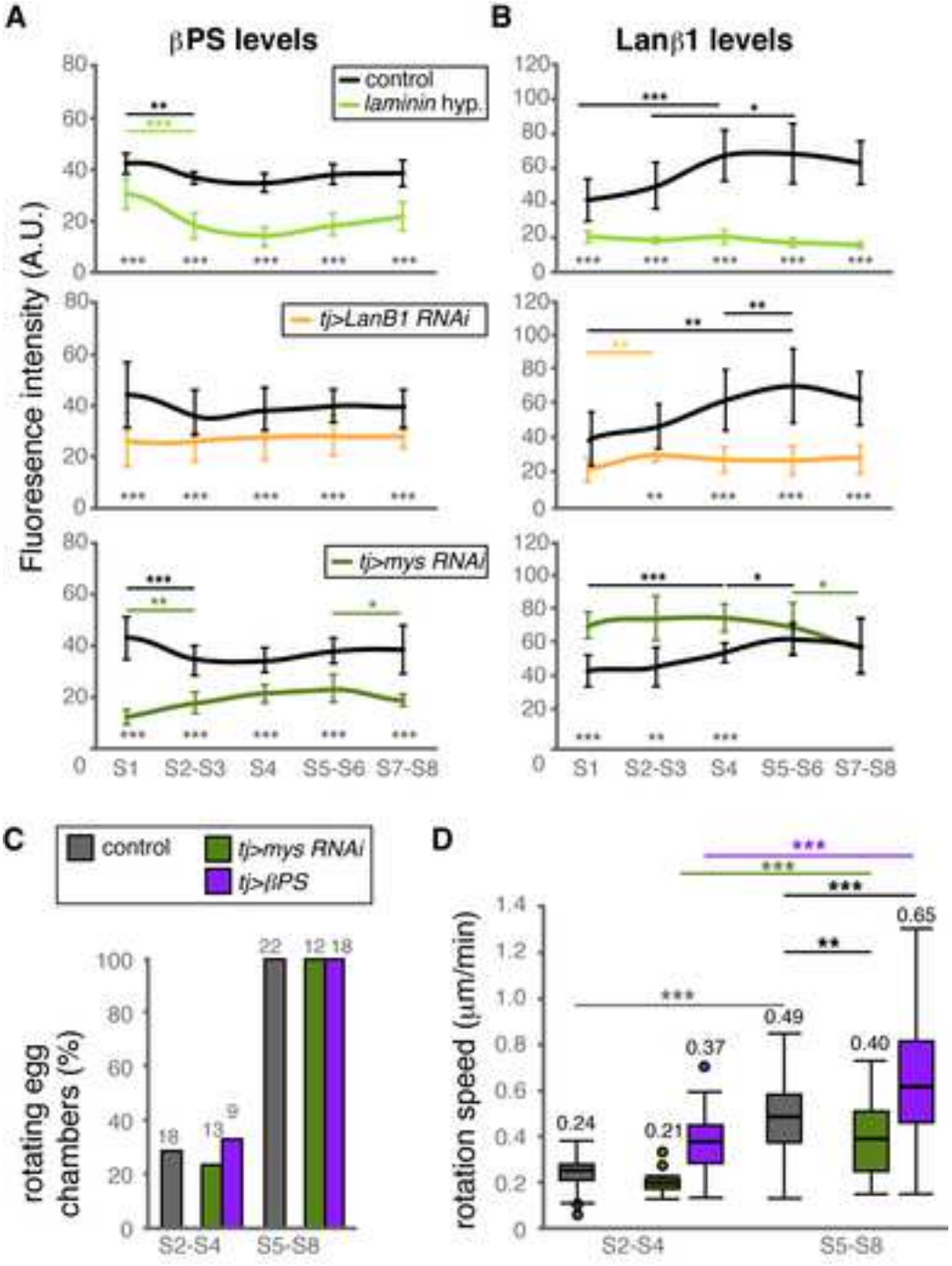

Figure 4

Fig. 5

Click here to download Figure Figure5_misp oo fixed-7.tif

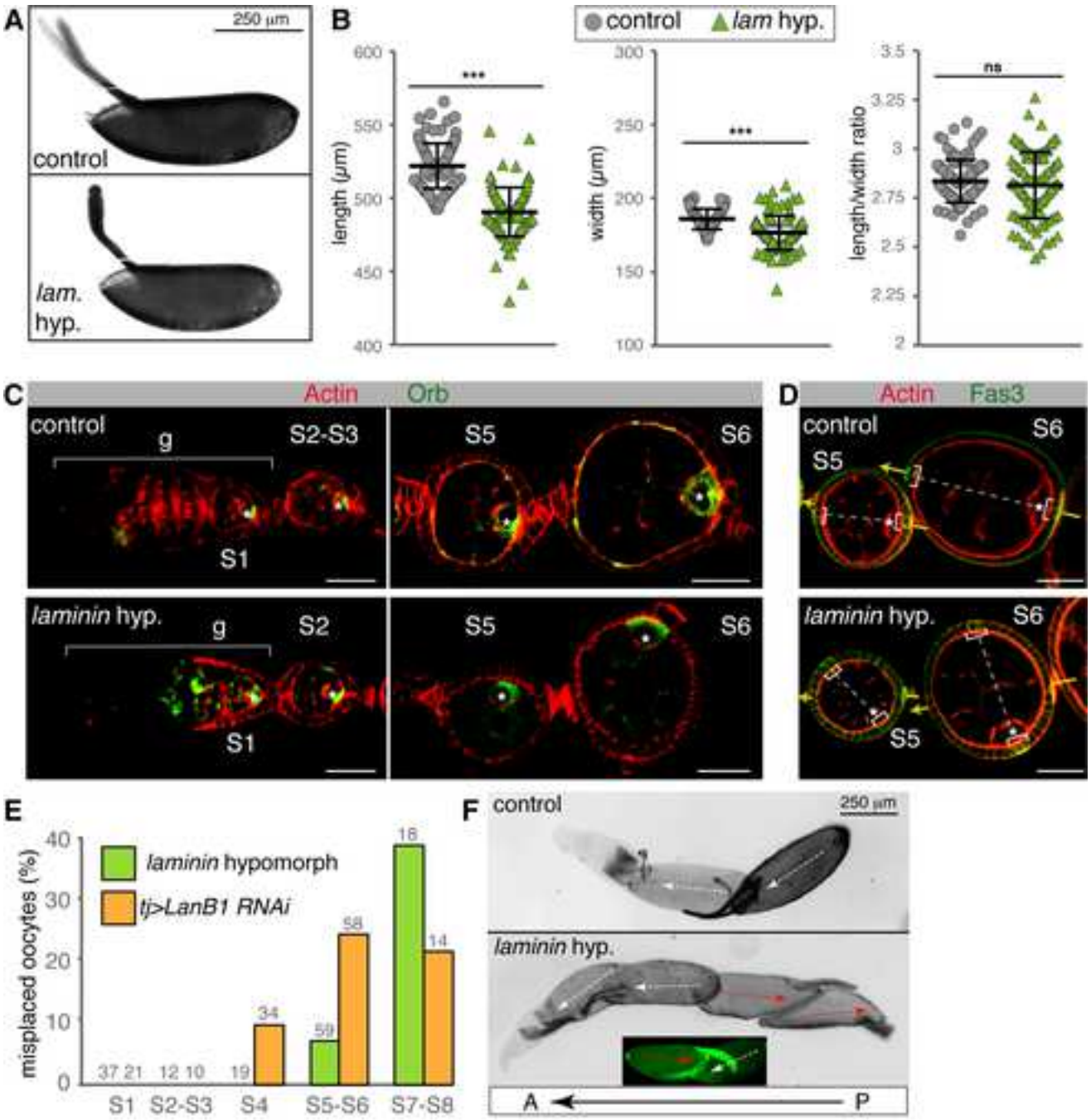

Figure 5

Fig. 6

Click here to download Figure Figure6_pc and stalk-6.tif

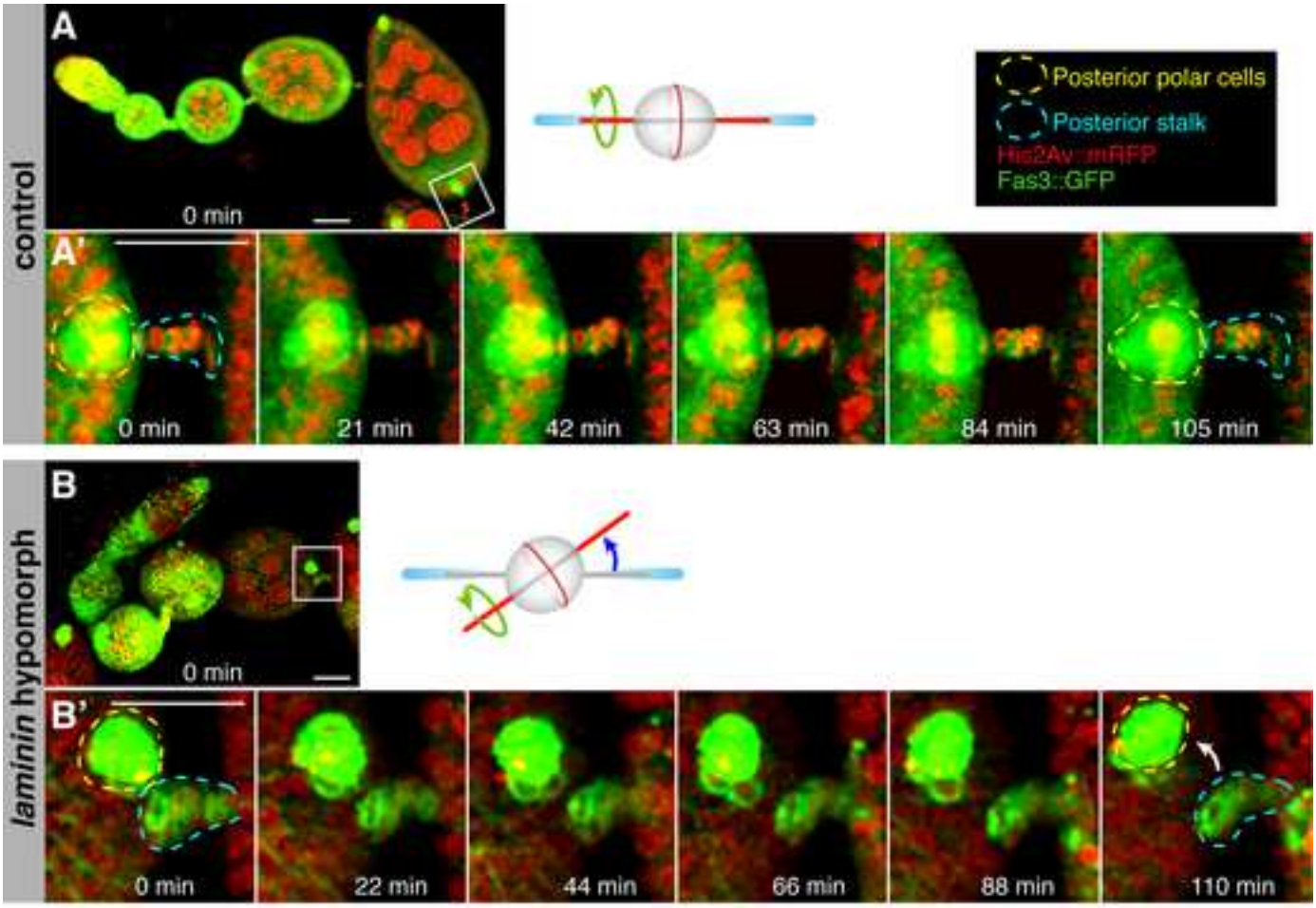

Figure 6

Fig. 7

Click here to download Figure Figure7_misp oo live-4.tif

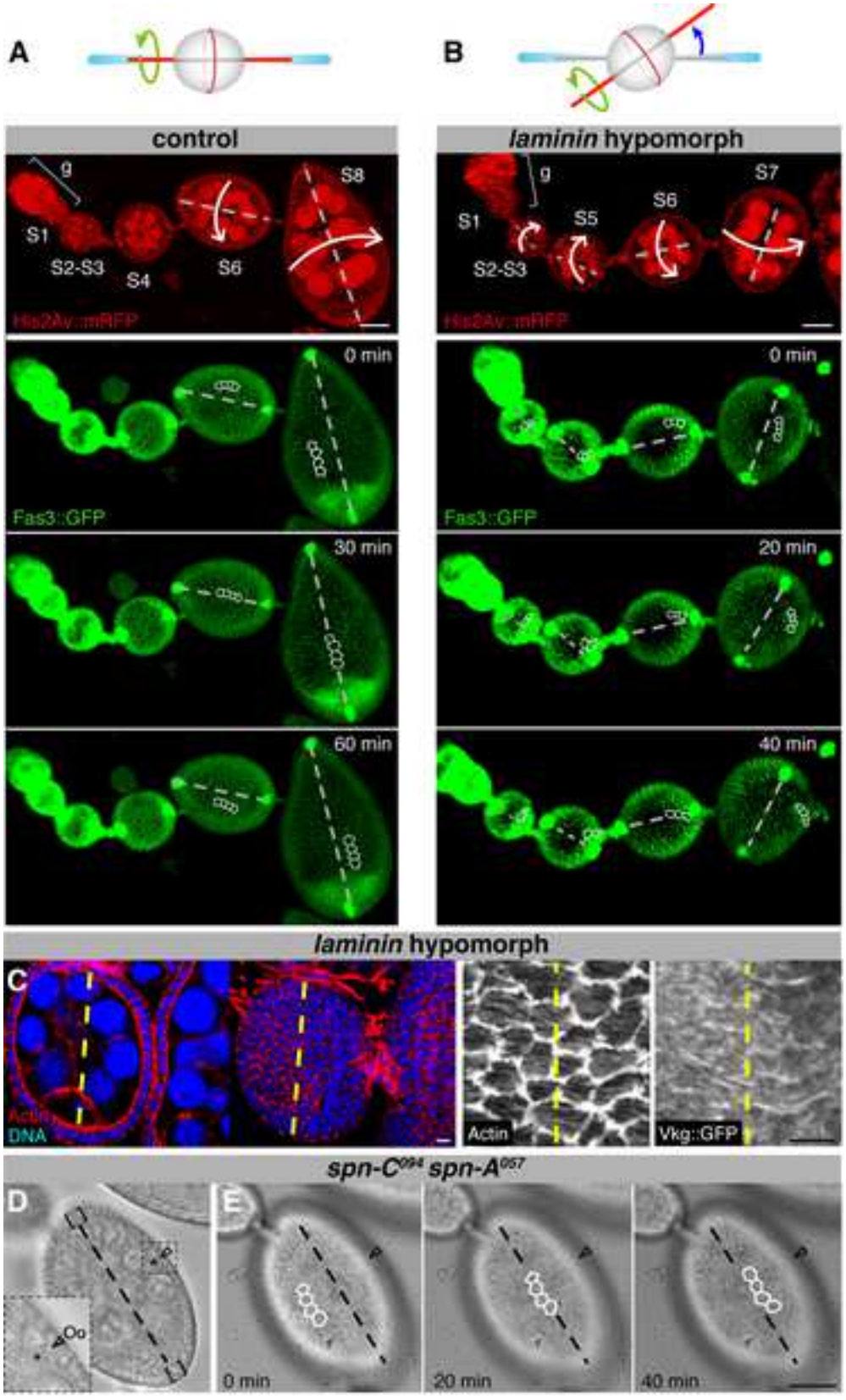

Figure 7

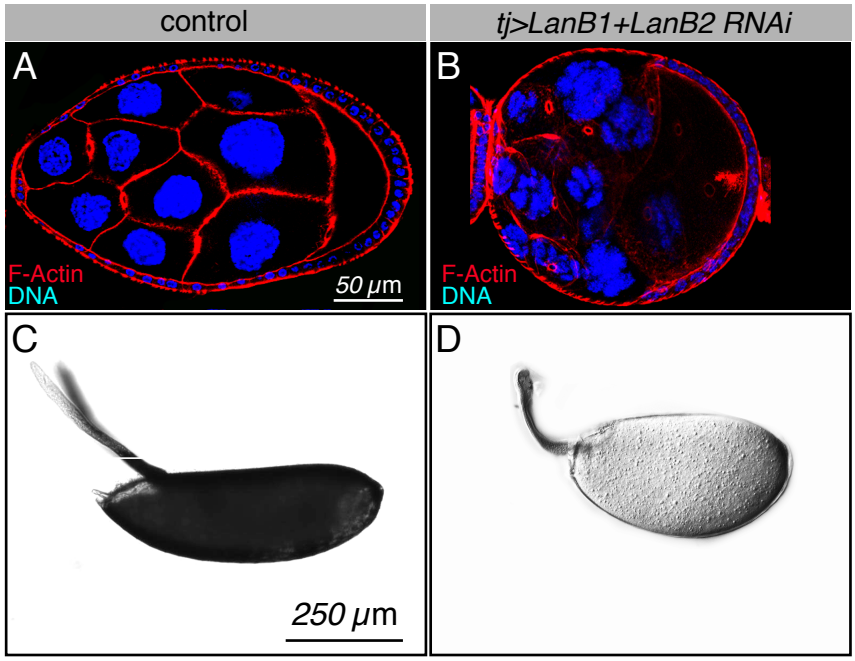

Supplemental Figure 1

Supplemental Figure 1 (related to Figures 1 and 2): Strong laminin depletion blocks egg elongation and follicle migration. (A) S5-S7 wild-type egg chambers are elongated along the anterior-posterior axis. **(B)** Strong depletion of laminin levels in *tj>LanB1+LanB2 RNAi* ovaries prevents egg elongation. Thus, S5-S7 egg chambers appear rounded (100% of cases, n=54). **(C)** The large majority of eggs laid by control females are properly elongated (number of eggs analysed (n)=178; length/width ratio ~2.75). **(D)** *tj>LanB1+LanB2 RNAi* females lay 86% eggs rounder than controls (n=89; length/width ratio <2.5). Filamentous actin was detected with rhodamine-labelled phalloidin.

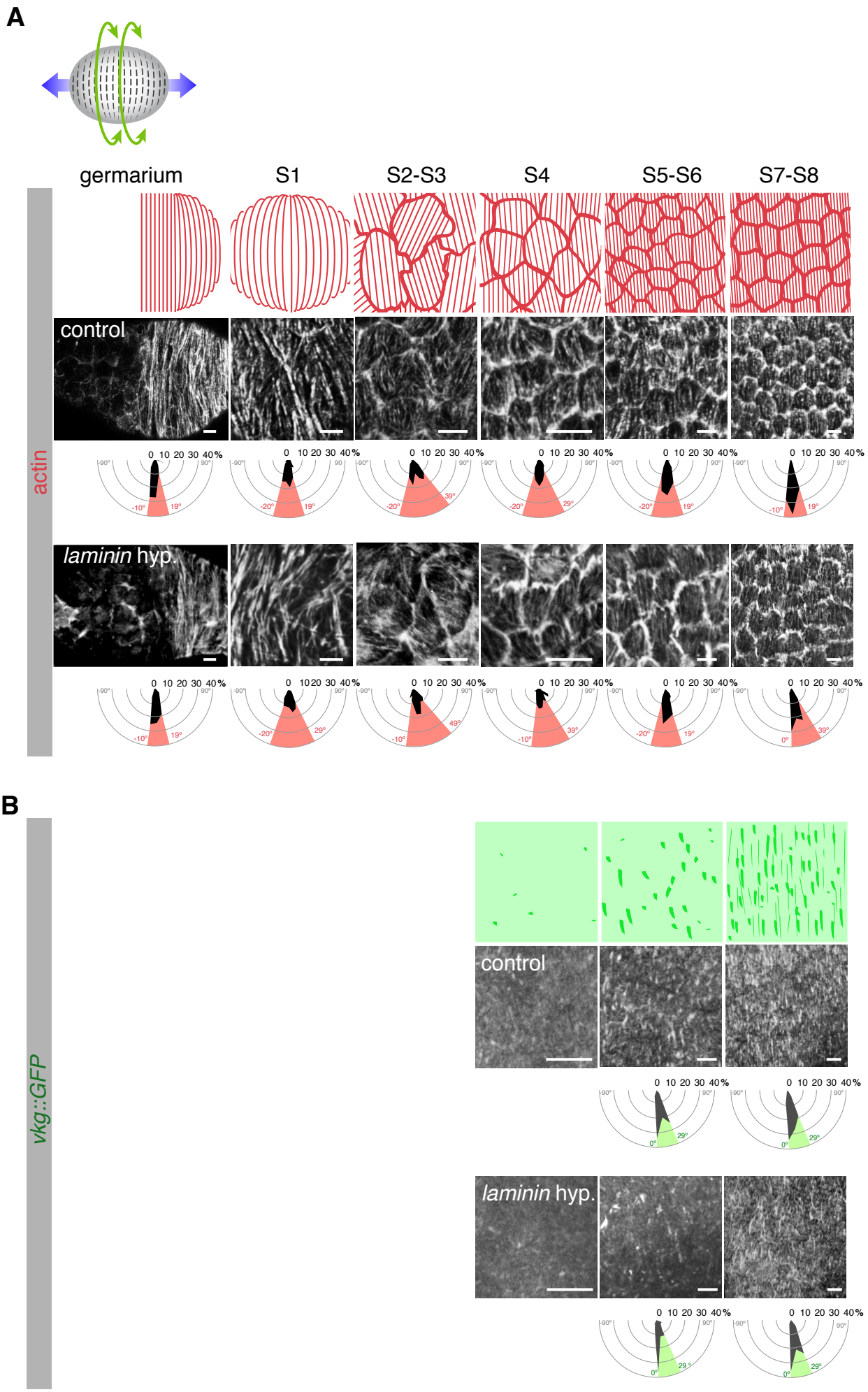

Supplemental Figure 2

Supplemental Figure 2 (related to Figure 2): Basal planar cell polarity of follicle cells and organisation of Col IV fibrils is not affected in *laminin* hypomorphic ovarioles. (A) Schematic representation of the distribution of basal actin filaments in follicle cells during egg chamber development (top). Visualisation of filamentous actin with rhodamine-labelled phalloidin in control (middle) and *laminin* hypomorphic ovarioles (bottom). Actin filaments are clearly organised perpendicular to the anterior-posterior axis of the ovariole in germarial stages and from S5 to S8. S2-S4 egg chambers display a less obvious polarisation. Radial diagrams indicate the percentage of bundles found within a given sector. The black areas correspond to the data reported in Table S2. Angles delimiting the sectors (depicted in pink) are shown. **(B)** Schematic representation of the organisation of the basement membrane component Col IV (top). Immunodetection of the protein trap Vkg::GFP in control (middle) and *laminin* hypomorphic ovarioles (bottom) show that Collagen IV is polarised perpendicular to the ovariole's AP axis from S5. Radial diagrams indicate the percentage of fibrils found within a given sector. The black areas correspond to the data reported in Table S4. Scale bars = 5 microns.

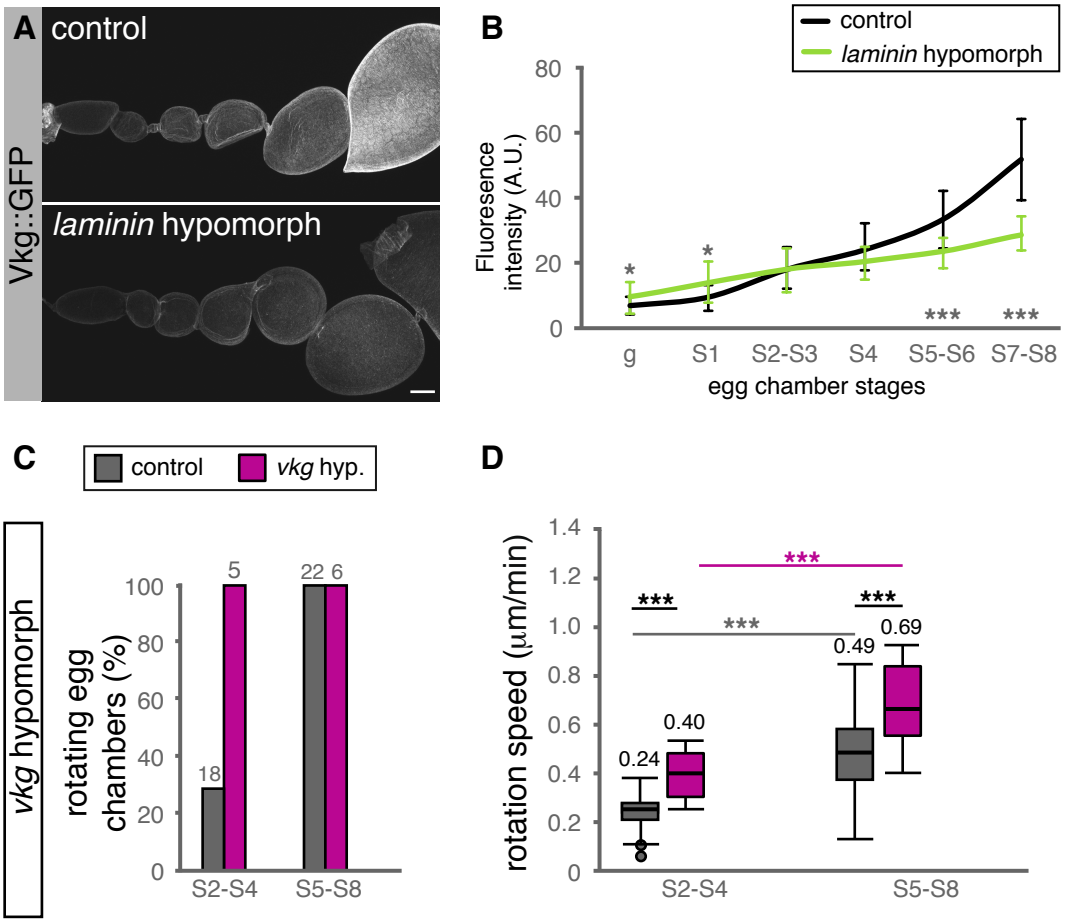

Supplemental Figure 3

Supplemental Figure 3 (related to Figure 2): Col IV deposition is affected in S7-8 *laminin* hypomorphs. Col IV is required for proper rotation. (A) Immunodetection of Col IV by means of the protein trap Vkg::GFP in control and *laminin* hypomorphic ovarioles using an anti-GFP antibody. Image is a maximum projection of at least 15 sections along the Z-axis. **(B)** Quantification of the immunofluorescence signal in different egg chambers is shown. Mean and standard deviation of measurements in 3 to 5 ovarioles are indicated. **(C)** Onset of rotation and **(D)** quantification of rotation speed of *vkg* hypomorphic follicles at different stages. Horizontal lines in boxes represent MEDIAN values of a minimum of 11 and a maximum of 103 measurements per genotype and stage. Values above boxes indicate MEAN rotation speeds. See Movies S1 and S7. P values of two-tailed t-tests <0.05 were considered statistically significant (*: P<0.05, **: P<0.005, ***: P<0.001). Scale bar = 25 microns.

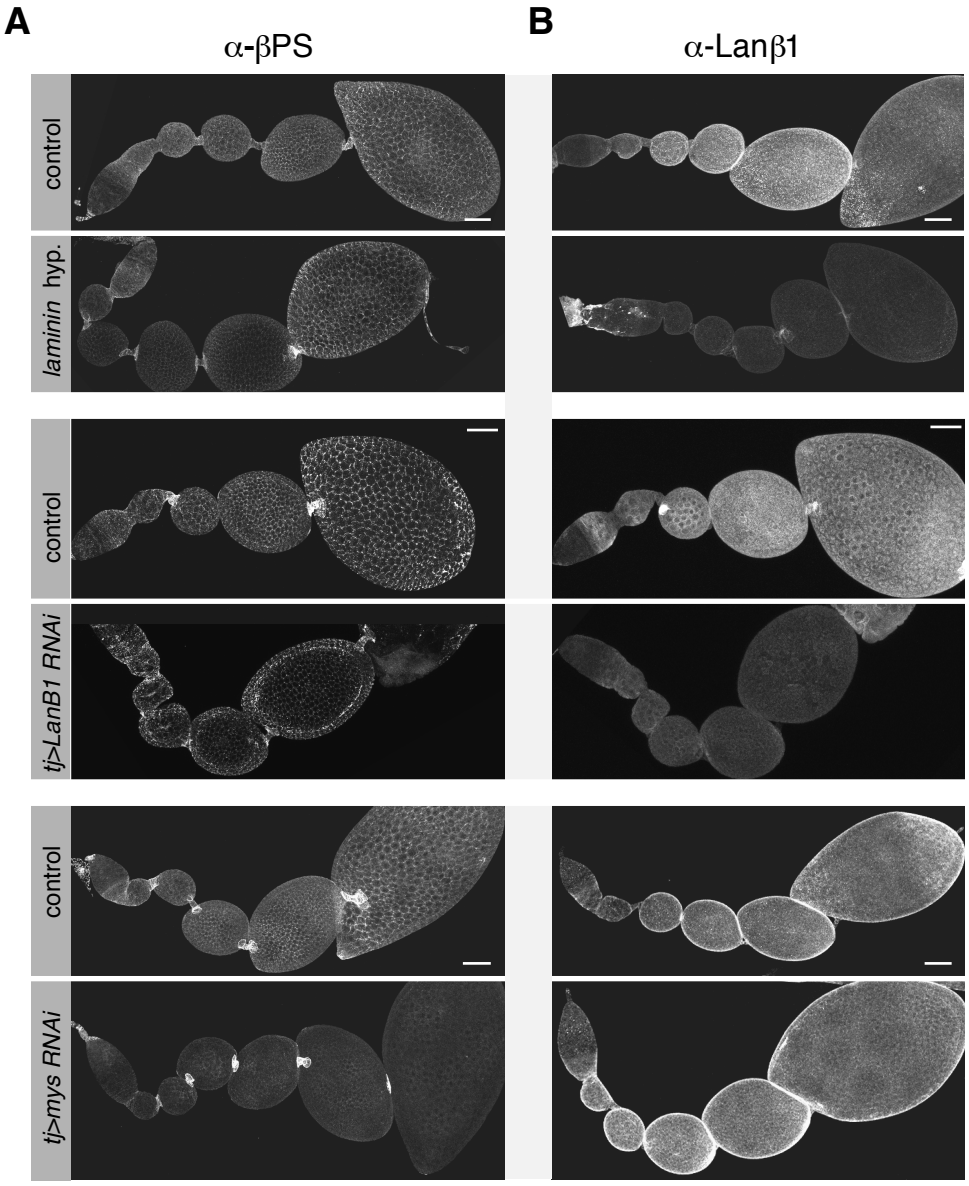

Supplemental Figure 4

Supplemental Figure 4 (related to Figure 4): **Visualisation of ßPS integrin and Laminin ß1 in control and experimental ovarioles. (A)** Immunodetection of ßPS and **(B)** Laminin ß1 during oogenesis in controls and in different genetic backgrounds. See Supplementary Table 1 for the quantification of fluorescence data. Images are maximum projections of at least 15 sections along the Z axis. Scale bars = 25 microns.

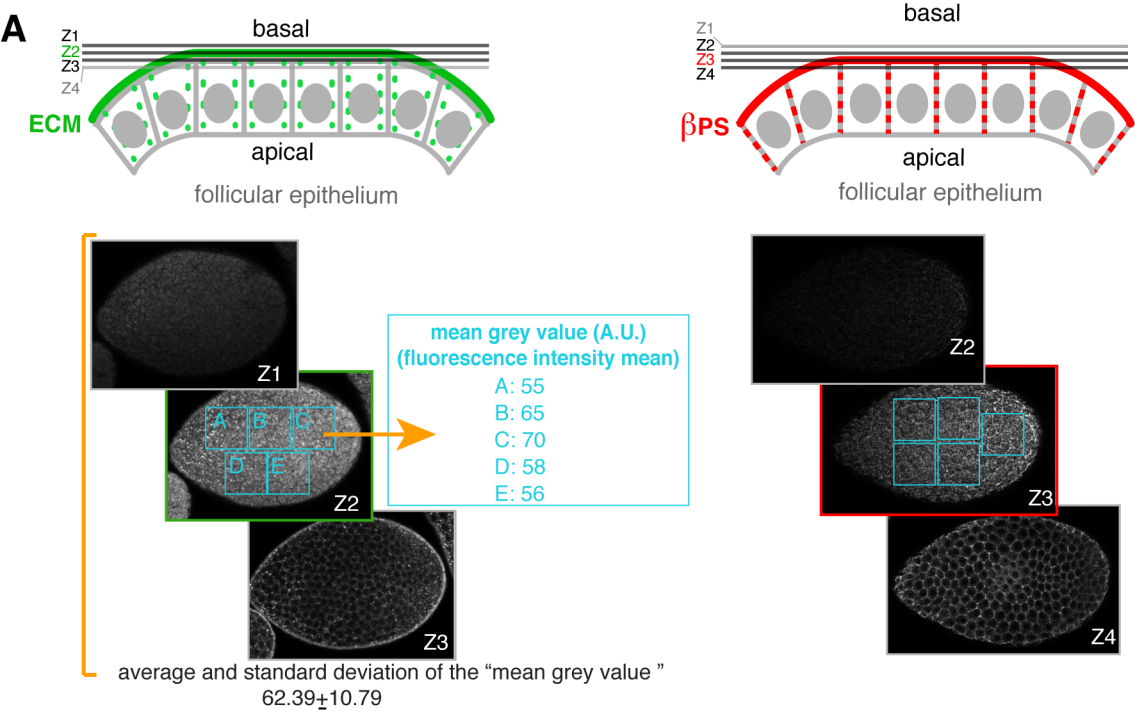

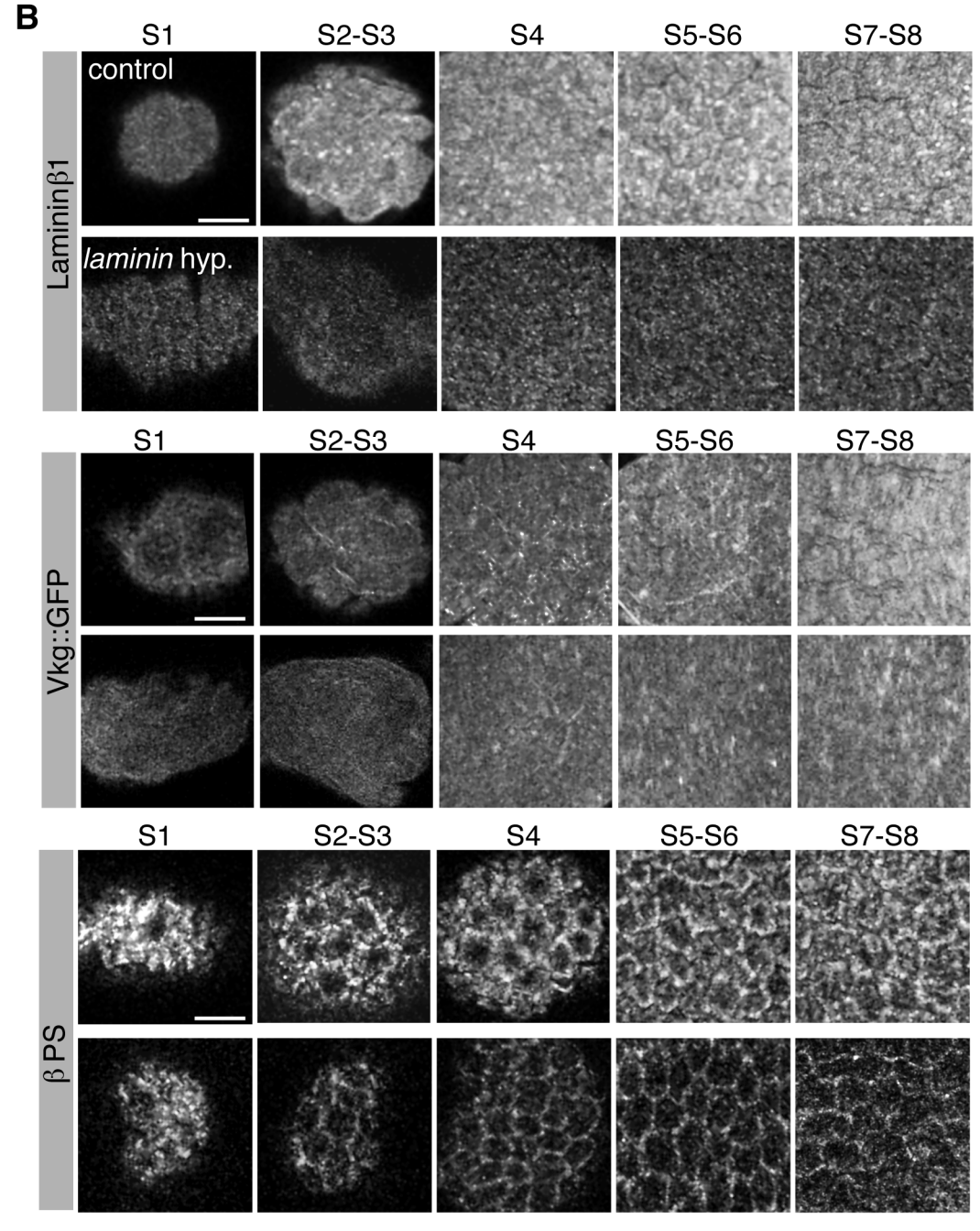

Supplemental Figure 5

Supplemental Figure 5 (related to Figures 1, 4, S3 and S4): **Quantification of immunofluorescence of basement membrane components and basal integrin**. **(A)** Schematic representation of the focal planes used to quantify immunofluorescence levels of BM components (green, left) and basal integrin (red, right). Confocal sections were taken through the egg chamber at 0.8-1.0 μm intervals (Z1, Z2, Z3 and Z4). Z2 cut through the plane of the BM (green line; to quantify ECM components). Membrane or cytoplasmic signals (green dashed lines) were discarded in BM measurements. Z3 focused on the basal side of the follicle cells (red line; to quantify integrin levels). Fluorescent signal from the lateral membrane of follicle cells (red dashed lines) was avoided in integrin measurements. For a given confocal section, five non-overlaping flat areas (cyan squares) were chosen to avoid edge effects and their mean "grey value" was calculated for each area using Imaris and/or ImageJ software (as shown for the BM example in **A**; see Suppl. Experimental Procedures for further details). Average fluorescence intensities ± standard deviations were calculated from ≥3 egg chambers of the appropriate stage (i. e., at least 15 measurements per stage). **(B)** Examples of high magnification images of basal laminin, Col IV and integrin immunofluorescence used for the analyses of protein levels in both control and experimental S1-S8 egg chambers. Scale bar = 5 microns.

SUPPLEMENTAL TABLE 1 (related to Figs. 1, 2, 4, S3 and S4)

Quantification of the immunofluorescence signal (A.U.) of Vkg::GFP, α-βPS and α-Laminin β1, and of rotation speed during oogenesis

genotype	egg chamber stage					
	germarium	**S1**	**S2-S3**	**S4**	**S5-S6**	**S7-S8**
collagen IV levels						
control	**6.10**±2.41	**9.15**±4.46	**17.91**±7.00	**24.05**±7.07	**33.34**±8.82	**52.00**±13.02
laminin hypomorph	**8.86**±4.72	**13.77**±6.19	**18.12**±6.29	**20.00**±5.59	**22.90**±4.70	**28.50**±5.26
fold change	*1.45*	*1.50*	*1.01*	*0.83*	*0.67*	*0.55*
	*	*			***	***
laminin levels						
control	**21.66**±3.63	**41.01**±15.3	**48.78**±12.7	**67.91**±5.84	**67.42**±21.86	**62.39**±10.79
laminin hypomorph	**22.82**±3.12	**21.53**±4.31	**19.51**±1.63	**20.58**±3.66	**17.66**±2.13	**16.60**±2.80
fold change	*1.05*	*0.53*	*0.40*	*0.31*	*0.26*	*0.27*
		***	***	***	***	***
control	**21.81**±3.63	**40.42**±13.6	**46.53**±11.3	**59.78**±15.31	**66.98**±18.74	**60.57**±13.40
tj>LanB1 RNAi	**13.65**±4.32	**21.82**±7.62	**31.03**±4.00	**28.31**±9.06	**27.54**±9.18	**28.76**±8.02
fold change	*0.63*	*0.54*	*0.67*	*0.47*	*0.41*	*0.47*
	***	***	***	***	***	***
control	**27.20**±2.05	**43.29**±9.58	**46.01**±11	**53.83**±5.65	**61.55**±9.09	**57.42**±15.42
tj>mys RNAi	**28.21**±4.48	**69.49**±7.81	**73.54**±12.7	**74.04**±8.33	**67.62**±14.91	**56.08**±16.67
fold change	*1.04*	*1.61*	*1.60*	*1.38*	*1.10*	*0.98*
		***	**	***		
integrin levels						
control	**12.00**±5.42	**42.24**±4.40	**36.93**±2.26	**34.79**±3.52	**38.15**±4.02	**38.32**±5.16
laminin hypomorph	**12.20**±2.86	**30.77**±5.49	**18.75**±5.17	**14.77**±4.77	**18.88**±4.19	**21.30**±5.70
fold change	*1.02*	*0.73*	*0.51*	*0.42*	*0.49*	*0.56*
		***	***	***	***	***
control	**14.53**±6.27	**44.44**±13.1	**36.86**±9.98	**38.55**±8.42	**39.85**±6.57	**39.39**±7.52
tj>LanB1 RNAi	**13.71**±3.91	**26.48**±10.9	**26.76**±8.77	**27.98**±9.33	**28.34**±8.21	**27.95**±3.78
fold change	*0.69*	*0.60*	*0.73*	*0.76*	*0.78*	*0.78*
		***	***	***	***	***
control	**19.20**±3.11	**43.10**±8.31	**34.54**±5.67	**34.22**±4.77	**38.06**±5.09	**38.20**±9.63
tj>mys RNAi	**20.72**±5.16	**12.90**±2.96	**18.41**±4.30	**22.18**±3.81	**24.02**±5.33	**19.88**±2.45
fold change	*1.08*	*0.30*	*0.53*	*0.65*	*0.63*	*0.52*
		***	***	***	***	***

Rotation speed (µm/min)	**S2-S4**	**S5-S8**
control	**0.24**±0.08	**0.49**±0.17
laminin hypomorph	**0.56**±0.18	**0.62**±0.27
tj>LanB1 RNAi	**0.50**±0.09	**0.79**±0.16
viking hypomorph	**0.40**±0.10	**0.69**±0.16
tj>mys RNAi	**0.21**±0.06	**0.40**±0.16
*tj>**βPS***	**0.37**±0.17	**0.65**±0.26

The fold change in fluorescence levels between mutant and control egg chambers is shown. Mean and standard deviation of a minimum of 11 and a maximum of 103 measurements per genotype and stage are indicated. See Supplementary Fig. 4 for examples of the original data. P values <0.05 were considered statistically significant (*:P<0.05, **:P<0.005, ***:P<0.001).

SUPPLEMENTAL TABLE 2 (related to Fig. S2)

Actin bundle alignment with respect to the AP axis (%)

genotype	angle (°)	egg chamber stage					
		germarium	S1	S2-S3	S4	S5-S6	S7-S8
control							
	-90 -81	2.96	0	0	0	0	0
	-80 -71	1.48	0.57	0	0	0	0
	-70 -61	0.00	1.14	1.61	0.56	0	0
	-60 -51	0.00	2.84	1.08	1.12	0	0
	-50 -41	0.00	1.70	1.08	2.25	0	1.61
	-40 -31	2.22	3.41	3.76	2.25	0.83	1.61
	-30 -21	3.70	7.39	5.38	6.74	6.67	0.54
	-20 -11	8.15	15.91	11.83	10.11	12.50	2.69
	-10 1	26.67	15.34	17.74	14.04	22.50	27.42
	0 9	26.67	19.32	9.68	18.54	25.00	39.25
	10 19	10.37	12.50	13.98	14.61	16.67	21.51
	20 29	5.19	5.68	15.59	10.11	5.83	4.30
	30 39	1.48	6.82	11.83	6.18	4.17	1.08
	40 49	0.74	2.84	4.84	5.62	0.83	1.61
	50 59	1.48	2.27	1.08	3.37	0.83	1.61
	60 69	8.89	1.70	0.54	2.25	2.50	0
	70 79	0.74	0.57	0	1.12	0.83	0
	80 90	0	0	0	0.56	0.83	0
***laminin* hypomorph**							
	-90 -81	0	1.19	0.58	0	0	0
	-80 -71	0	1.19	0.58	0.73	0	0
	-70 -61	0	8.33	0.58	2.92	0	0.60
	-60 -51	0	1.19	1.16	2.92	0	0.60
	-50 -41	1.12	1.19	1.16	2.19	0.58	0.91
	-40 -31	4.49	7.14	1.16	2.19	1.16	0.91
	-30 -21	5.62	4.76	2.89	5.11	5.78	0.91
	-20 -11	8.99	8.33	6.36	5.11	9.83	3.63
	-10 1	19.10	17.86	11.56	10.22	23.70	5.14
	0 9	24.72	17.86	11.56	13.14	20.23	29.61
	10 19	25.84	10.71	12.14	12.41	17.92	20.85
	20 29	7.87	10.71	15.61	8.03	6.36	23.26
	30 39	2.25	8.33	13.87	9.49	6.36	9.67
	40 49	0	1.19	10.40	2.92	4.05	2.42
	50 59	0	0	4.62	8.76	1.73	1.21
	60 69	0	0	2.31	7.30	0.58	0
	70 79	0	0	2.31	2.19	1.16	0
	80 90	0	0	0	2.19	0.58	0.30

Quantification of the relative angles of basal actin bundles of follicle cells. A 0° angle represents a bundle perpendicular to the AP axis. Values refer to the percentage of bundles with a given orientation with respect to the AP axis of the ovariole. Intervals that contain at least 9.5% of the scored bundles are highlighted in red. A minimum of 100 bundles were analysed from at least 5 egg chambers per stage.

SUPPLEMENTAL TABLE 3 (related to Fig. S2)

Col IV fibril alignment with respect to the AP axis (%)

genotype	angle (°)	Egg chamber stage	
		S5-S6	S7-S8
control			
	-90 -81	*0*	*0*
	-80 -71	*0*	*0*
	-70 -61	*0*	*0*
	-60 -51	*0*	*0*
	-50 -41	*0*	*0*
	-40 -31	*0*	*1.44*
	-30 -21	*1.10*	*1.44*
	-20 -11	*4.40*	*2.01*
	-10 1	*7.69*	*8.91*
	0 9	*32.97*	*34.48*
	10 19	*19.78*	*27.30*
	20 29	*24.18*	*19.25*
	30 39	*5.49*	*4.89*
	40 49	*3.30*	*0.29*
	50 59	*1.10*	*0*
	60 69	*0*	*0*
	70 79	*0*	*0*
	80 90	*0*	*0*
***laminin* hypomorph**			
	-90 -81	*0*	*0*
	-80 -71	*0*	*0*
	-70 -61	*0*	*0*
	-60 -51	*0*	*0*
	-50 -41	*0*	*0.58*
	-40 -31	*0*	*0.58*
	-30 -21	*3.90*	*0.58*
	-20 -11	*2.60*	*2.89*
	-10 1	*6.49*	*5.20*
	0 9	*36.36*	*36.42*
	10 19	*12.99*	*20.81*
	20 29	*12.99*	*24.86*
	30 39	*7.79*	*8.09*
	40 49	*5.19*	*0*
	50 59	*3.90*	
	60 69	*3.90*	*0*
	70 79	*3.90*	*0*
	80 90	*0*	*0*

Quantification of the relative angles of Collagen IV:GFP fibrils. A 0° angle represents a fibril perpendicular to the AP axis. Values refer to the percentage of fibrils with a given orientation with respect to the AP axis of the ovariole. Intervals that contain at least 10% of the scored bundles are highlighted in green. A minimum of 50 fibrils were analysed from at least 5 egg chambers per stage.

SUPPLEMENTAL EXPERIMENTAL PROCEDURES

Experimental genotypes

Figure 1
control: *w*; *ubi-GFP FRT40/CyO*
laminin hypomorph: *w/w; l(2)k05404/LanB1^{28a}*
tj>LanB1 RNAi: UAS-dicer/+; tj-Gal4/+; UAS-LanB1 RNAi/tub-Gal80^{ts}

Suppl. Figure 1
tj>LanB1+LanB2 RNAi: UAS-dicer/+; tj-Gal4/UAS-LanB2 RNAi; UAS-LanB1 RNAi/tub-Gal80^{ts}

Figure 2; Suppl. Movies S1 and S2
control: *w*; *Fas3::GFP/+*; *His2Av::mRFP/+*
laminin hypomorph: *w*; *l(2)k05404 Fas3::GFP/LanB1^{28a} His2Av::mRFP*
tj>LanB1 RNAi: UAS-dicer/+; tj-Gal4/+; UAS-LanB1 RNAi/tub-Gal80^{ts}

Suppl. Figures S2 and S3
control: *w*; *l(2)k05404, vkg::GFP/+; +/TM2*
laminin hypomorph: *w*; *l(2)k05404, vkg::GFP/LanB1^{28a} His2Av::mRFP*
viking hypomorph: y *w*/+; *vkg^{01209}/ vkg^{K07138}; ry[506]/+*

Figure 3
control: *w*; *ubi-GFP FRT40/CyO*
laminin hypomorph: *w/w; l(2)k05404/LanB1^{28a}*

Figure 4; Suppl. Figure 4; Suppl. Movie S2
control: *w*; *ubi-GFP FRT40/CyO*
control: *w*; *Fas3::GFP/+*; *His2Av::mRFP/+*
laminin hypomorph: *w/w; l(2)k05404/LanB1^{28a}*
laminin hypomorph: *w*; *(l)2k05404 Fas3::GFP/LanB1^{28a} His2Av::mRFP*
tj>LanB1 RNAi: UAS-dicer/+; tj-Gal4/+; UAS-LanB1 RNAi/tub-Gal80^{ts}
tj>mys RNAi: w; UAS-mys RNAi/tj-Gal4; tub-Gal80^{ts}/+
tj>βPS: UAS-βPS/ traffic jam-Gal4; tub-Gal80^{ts}/+
tj>LanB1 RNAi+βPS (control): UAS-dicer/+; tj-Gal4/UAS-GFP; UAS-LanB1 RNAi/tub-Gal80^{ts}
tj>LanB1 RNAi+βPS: UAS-dicer/+; tj-Gal4/UAS-βPS; UAS-LanB1 RNAi/tub-Gal80^{ts}

Figure 5
control: *w*; *ubi-GFP FRT40/CyO*
laminin hypomorph: *w/w; l(2)k05404/LanB1^{28a}*
tj>LanB1 RNAi: UAS-dicer/+; tj-Gal4/+; UAS-LanB1 RNAi/tub-Gal80^{ts}

Figure 6; Suppl. Movies S4-6
control: *w*; *Fas3::GFP/+*; *His2Av::mRFP/+*
laminin hypomorph: *w*; *l(2)k05404 Fas3::GFP/LanB1^{28a} His2Av::mRFP*
tj>lanB1 RNAi+GFP (control): UAS-dicer/+; tj-Gal4/tub-Gal80^{ts}; UAS-LanB1 RNAi/UAS-GFP
tj>lanB1 RNAi+Abi RNAi: UAS-dicer/+; tj-Gal4/tub-Gal80^{ts}; UAS-LanB1 RNAi/UAS-Abi RNAi

Figure 7; Suppl. Movie S7
control: *w*; *Fas3::GFP/+*; *His2Av::mRFP/+*
laminin hypomorph: *w*; *l(2)k05404 Fas3::GFP/LanB1^{28a} His2Av::mRFP*
spindle mutant egg chamber from a homozygous female: *w;; ru spn-C^{094} e spn-A^{057} ca*

Immunohistochemistry

Primary antibodies were used at the following concentrations: rabbit anti-Laminin b1 (Kumagai et al., 1997), 1:1000; FITC-conjugated anti-GFP (Abcam, ab6662), 1:500; anti-Fasciclin3 mouse monoclonal, 1:50 (7G10 anti-Fasciclin III was deposited to the DSHB by Goodman, C.); anti-orb mouse monoclonal, 1:10 (a mixture of Orb 4H8 and Orb 6H4 monoclonal antibodies, 1:20 each; 4H8 and 6H4 anti-Orb were deposited to the DSHB by

Schedl, P.); anti-bPS mouse monoclonal, 1:100 (CF.6G11 anti-βPS was deposited to the DSHB by Brower, D.).

Imaging of ovarian tissues

3-D images of fixed samples were acquired using a 40x/1.3 NA oil immersion objective. 4-D *in vivo* images were acquired at room temperature (~20ºC). We used a Leica SP5 confocal microscope controlled by the Leica LAS AF software. To analyse rotation, we performed live imaging of complete ovarioles using a 20x/0.7 NA oil immersion objective and Leica hybrid detectors (standard mode), with time points every 2-4 minutes for 1-6 hours. Follicle cell migration was analysed either with the Fas3::GFP and His2Av::mRFP fluorescence proteins or with transmitted light (phase contrast). Rendering of 4-D live images were performed in Imaris. Snapshots were obtained and processed using ImageJ and Adobe Photoshop, and labelled in Adobe Illustrator.

Transmission Electron Microscopy (TEM)

Ovaries were dissected in Phosphate Buffer Saline + 0.1% Tween-20 and fixed for 2 hours at 4 ^{0}C in 3% glutaraldehyde/l% paraformaldehyde (vol./vol.) in 0.05 M cacodylate buffer (pH 7.4). After three 10 min. washes in cacodylate buffer 0.1 M at 4 ^{0}C, ovaries were postfixed for 1 hour at 4ºC in darkness in 1% OsO_4, 1% $K_3Fe[CN]_6$ in water. After three rinses in distilled water at 4ºC, ovaries were stained for 2 hours at room temperature (RT) in darkness in 0.5% uranyl acetate, rinsed again in distilled water and dehydrated through an ethanol rising series (50%, 70%, 90% and 3x100%; 10 min. each) at RT and infiltrated with Embed 812 resin (Electron Microscopy Sciences). The resin-embedded specimens were polymerized by incubation in fresh Embed 812 during 48 hours at 60 ^{0}C in flat plastic embedding molds, which were cut in 50-70 nm thick sections with a DIATOME diamond-blade fixed on a Reichert Jung Ultramicrotome and mounted on copper grids. Sections were counterstained with 1% uranyl acetate in 50% ethanol for 1 min. and then stained with lead citrate for 5 minutes in a CO_2-free atmosphere. Sections were examined with a Zeiss EM902 electron microscope at 80Kv, and photographed at 50.000x magnification.

Atomic Force Microscopy measurements

Ovarioles were dissected out of the muscle sheath to make sure that the AFM cantilever was in direct contact with the basement membrane. Stiffness of *ex-vivo* ovarian tissues immobilized on Petri dishes using Cell-Tak (BD Biosciences, Oxford, UK) and containing *Drosophila* culture media was tested by AFM within 30 minutes of dissection. Monodisperse polystyrene beads (diameter 5.46 ± 0.12 μm, microParticles GmbH, Berlin, Germany) were glued to silicon cantilevers with a nominal spring constant of 0.1 N/m (PPP-BSI, Nanosensors, Neuchatel, Switzerland). Cantilevers were mounted on a JPK Nanowizard Cellhesion 200 (JPK Instruments AG, Berlin, Germany) set up on an inverted optical microscope. Exact cantilever spring constants were determined using the thermal noise method included in the AFM software. Freshly dissected samples were measured under visual control (Franze et al., 2011). Force-distance-curves were taken at an approach speed of 10 μm/s and a maximum force F = 6 nN. Force–distance curves were analyzed for an indentation depth d = 0.2 μm using a custom algorithm based in Matlab (Christ et al., 2010) (MathWorks, Natick, USA), which fits the Hertz model to the data: $F = \frac{4}{3} K \sqrt{R} \delta^{3/2}$, where the apparent elastic modulus $K = \frac{E}{1-\nu^2}$ is a measure of elastic stiffness, R is the radius of the indenter, E is the Young's modulus, and n is the Poisson's ratio. Normal distribution of AFM measurements was confirmed using the Kolmogorov-Smirnov test. The statistical significance of the differences between experimental and control values was evaluated using two-tailed t-tests. 58 measurements from 11 control ovarioles and 48 from 10 *laminin* mutants were collected.

Quantification of migration speed and fluorescent levels

The tracking of individual cells was performed using Fasciclin3::GFP (Fas3::GFP), Histone2Av::RFP (His2Av:mRFP) or transmitted light (Movies S1-S11). Lineal velocity of follicle cells was calculated by manually tracking nuclei or geometrical cell centres using the Leica LAS AF software, which allowed precise determination of time and length of movement. Dispersion of the migration speed data was represented using box-plot graphs, where the median and the outliers are indicated.

To quantify fluorescence in control and experimental samples and to avoid unwanted variability, both genotypes were dissected in parallel and fixed and immunostained in the same tube. To distinguish between experimental and control samples in a given experiment, we expressed a fluorescent marker (either nuclear GFP or His2Av::mRFP) in only one of the genotypes. In addition, quantification was performed on images captured using identical confocal settings. Z-sections were taken at 0.8-1.0 μm intervals. Colour depth was set to 12-bit and configured so that most of the pixels were within the dynamic range of the detectors. Z-Depth was selected manually and FITC, GFP or Cyanine5 fluorescence intensity signals were quantified in the plane of maximum

signal of the BM (laminin and Col IV) or of the basal surface of the follicle cells (integrin). Analysis was only done on consecutive egg chambers of ovarioles outside of the muscle sheath and from at least three biological replicas. Fluorescent intensity was measured in five different areas per 3+ egg chambers (Fig. S5). Image stacks were converted to grey scale and pre-processed using the standard background subtraction function of ImageJ (default settings; 50 pixel radius). Measurements were taken using IMARIS software with the "Measurement points" tool and/or the "ROI measurement" tool from the ImageJ software choosing the Z plane with maximal fluorescence signal. The "ROI measurement" tool allowed us to calculate the mean grey values for each area (Fig S5). Mean grey value equals the sum of the grey values of all the pixels in the selected area divided by the number of pixels and it is expressed in arbitrary units (A.U.). Egg chambers were staged according to (Spradling, 1993). Basically, we used the shape of the chamber, the morphology of the follicular epithelium and stalk cells, chromatin organisation in the nurse cells and the oocyte/nurse cells size ratio to assign the different stages.

Quantification of basal actin bundle and Col IV fibril alignment

One-plane confocal images were acquired and rotated to orientate the AP axis of the ovariole so that anterior is to the left. The orientation of both types of filaments was calculated by determining the angle between each filament and the AP axis of the ovariole (in the germarium and S1 follicles), or the axis defined by the polar cells (from S2-S8), using the line ROI tool of FIJI (Schindelin et al., 2012). Angular data was distributed from -90° to 90°, being 0° a perpendicular alignment. Angles were grouped in 10° intervals, and the percentage of filaments included within each interval was plotted as radial diagrams. Actin bundle alignment was determined from the germarium to S8 follicles; Col IV (*vkg::GFP*) fibrils were quantified in S5-S8 egg chambers.

SUPPLEMENTAL REFERENCES

Christ, A.F., Franze, K., Gautier, H., Moshayedi, P., Fawcett, J., Franklin, R.J., Karadottir, R.T., and Guck, J. (2010). Mechanical difference between white and gray matter in the rat cerebellum measured by scanning force microscopy. Journal of biomechanics 43, 2986-2992.

Franze, K., Francke, M., Günter, K., Christ, A.F., Körber, N., Reichenbach, A., and Guck, J. (2011). Spatial mapping of the mechanical properties of the living retina using scanning force microscopy. Soft Matter 7, 3147.

Kumagai, C., Kadowaki, T., and Kitagawa, Y. (1997). Disulfide-bonding between Drosophila laminin β and γ chains is essential for α chain to form αβγ trimer. FEBS Lett 412, 211-216.

Schindelin, J., Arganda-Carreras, I., Frise, E., Kaynig, V., Longair, M., Pietzsch, T., Preibisch, S., Rueden, C., Saalfeld, S., Schmid, B., et al. (2012). Fiji: an open-source platform for biological-image analysis. Nat Meth 9, 676-682.

Spradling, A. (1993). Developmental genetics of oogenesis. In The Development of Drosophila melanogaster, M. Bate, and A. Martinez-Arias, eds. (New York: Cold Spring Harbor Laboratory press), pp. 1-70.

Suppl. Movie 1

Suppl. Movie 2

Suppl. Movie 3

Click here to access/download

Supplemental Movies and Spreadsheets

Fig4_S3movie_tjlanB1ibPS-2.mov

Suppl. Movie 4

Click here to access/download

Supplemental Movies and Spreadsheets

Fig6 and 7_S4movie_pc control.mov

Suppl. Movie 5

Suppl. Movie 6

Click here to access/download

Supplemental Movies and Spreadsheets

Fig7_S6movie_pc lam hyp.mov

Suppl. Movie 7

Click here to access/download

Supplemental Movies and Spreadsheets

Fig7_S7movie_spnCA.mov